

Minimization of AND-XOR Expressions with Decoders for Quantum Circuits

Sonia Yang^{*1}, Ali Al-Bayaty^{†1}, and Marek Perkowski^{‡1}

¹*Department of Electrical and Computer Engineering, Portland State University, USA*

Abstract

This paper introduces a new logic structure for reversible quantum circuit synthesis. Our synthesis method aims to minimize the quantum cost of reversible quantum circuits with decoders. In this method, multi-valued input, binary output (MVI) functions are utilized as a mathematical concept only, but the circuits are binary. We introduce the new concept of “Multi-Valued Input Fixed Polarity Reed-Muller (MVI-RM)” forms. Our decoder-based circuit uses three logical levels in contrast to commonly-used methods based on Exclusive-or Sum of Products (ESOP) with two levels (AND-XOR expressions), realized by Toffoli gates. In general, the high number of input qubits in the resulting Toffoli gates is a problem that greatly impacts the quantum cost. Using decoders decreases the number of input qubits in these Toffoli gates. We present two practical algorithms for three-level circuit synthesis by finding the MVI-FPRM: products-matching and the newly developed butterfly diagrams. The best MVI-FPRM forms are factorized and reduced to approximate Multi-Valued Input Generalized Reed-Muller (MVI-GRM) forms.

1 Introduction

Researchers in the area of quantum circuits and quantum compilers [1, 2] seek efficient methods to synthesize multi-output quantum reversible circuits [2–12]. Several classical methods can be adapted for quantum circuits. Some methods [13, 14] are based on binary Fixed-Polarity Reed-Muller (FPRM) forms. For a function of n variables, there are 2^n such canonical forms, and the synthesized quantum circuits corresponding to these forms can differ significantly in their quantum costs [15–17]. Such synthesis methods have also been extended to binary Generalized Reed-Muller (GRM) forms [18–21] to minimize the final quantum costs by minimizing the number of inputs to the Toffoli gates. Most of these methods attempt to minimize the number of many-input Toffoli gates. The idea of using decoders for classical Sum of Products (SOP) logic was invented by Tsutomu Sasao [22], and it is applied for the first time here to binary quantum circuits based on Exclusive-or Sum of Products (ESOP), also known as AND-XOR expressions. The FPRM and GRM forms are special cases of ESOP expressions, but GRM forms tend to be less cost-expensive compared with non-GRM ESOP expressions in terms of the number of many-input Toffoli gates. Using decoders minimizes the number of inputs to the Toffoli gates. This paper introduces the concept of a logic with multi-valued inputs, binary outputs for the synthesis of entirely binary quantum reversible circuits [23, 24].

This paper is organized as follows. Section 2 presents background information on Reed-Muller (RM) forms, expansions, reversible quantum gates, two definitions of quantum cost, and FPRM butterfly diagrams. Section 3 introduces multi-valued input, binary output (MVI) logic, and extends concepts from binary logic to MVI logic. Section 4 demonstrates how to realize a quantum circuit with decoders based on MVI-FPRM forms. Section 5 introduces a products-matching algorithm to find the MVI-FPRM of a function. Section 6 applies the products-matching algorithm and constructs two possible reversible quantum circuits with decoders for a two-bit adder. Section 7 introduces a butterfly diagram algorithm to find the MVI-FPRM of a function. Section 8 presents circuit synthesis based on MVI-GRM forms by factoring from MVI-FPRM forms. Lastly, Section 9 concludes the paper.

2 Background

This section provides background on binary Reed-Muller (RM) forms, Boolean expansions, quantum gates, quantum cost, and butterfly diagrams.

^{*}sonia.liu.yang@gmail.com

[†]albayaty@pdx.edu

[‡]h8mp@pdx.edu

2.1 Binary Reed-Muller Forms

There are many binary RM forms [13, 14, 18–21, 25]. In this paper, we focus on *Fixed-Polarity Reed-Muller (FPRM) forms* [13, 14] and *Generalized Reed-Muller (GRM) forms* [18–21]. This section gives background on the RM forms.

A literal in binary logic is either of positive (x) or negative (\bar{x}) polarity. The *Positive Polarity Reed-Muller (PPRM) form* is a special case of the FPRM form, where all literals are positive polarity, e.g., $1 \oplus x_1 \oplus x_2 \oplus x_1 x_2$ is a PPRM form, but $1 \oplus \bar{x}_1 \oplus x_2 \oplus x_1 x_2$ is not because \bar{x}_1 is negative polarity. It is formally defined in Definition 1.

Definition 1. The binary Positive Polarity Reed-Muller (PPRM) form of a single-output function $f(x_1, x_2, \dots, x_n)$ is the function in the form of Eq. (1), where all literals are of positive polarity and $a_i \in \{0, 1\}$.

$$f(x_1, x_2, \dots, x_n) = a_0 \oplus a_1(x_1) \oplus a_2(x_2) \oplus \dots \oplus a_{2^n-1}(x_1 x_2 \dots x_n) \quad (1)$$

□

The PPRM form can be generalized to the FPRM form, where each variable is assigned a polarity so that all literals of a certain variable are of the assigned polarity. For example, a function with polarity 101 (x_1 is positive polarity, x_2 is negative polarity, and x_3 is positive polarity) is $\bar{x}_2 \oplus x_1 \bar{x}_2 \oplus x_1 x_3$. The FPRM form is defined in Definition 2.

Definition 2. The binary Fixed Polarity Reed-Muller (FPRM) form of a single-output function $f(x_1, x_2, \dots, x_n)$ with polarity p_1, p_2, \dots, p_n , where $p_i \in \{0, 1\}$, is the function in the form of Eq. (2), where $a_i \in \{0, 1\}$.

$$\hat{x}_i = \begin{cases} \bar{x}_i & \text{if } p_i = 0 \\ x_i & \text{if } p_i = 1 \end{cases}$$

$$f(x_1, x_2, \dots, x_n) = a_0 \oplus a_1(\hat{x}_1) \oplus a_2(\hat{x}_2) \oplus \dots \oplus a_{2^n-1}(\hat{x}_1 \hat{x}_2 \dots \hat{x}_n) \quad (2)$$

□

GRM forms are not based on polarity and are instead based on the set of variables in each term. A GRM form is one where no pair of terms has exactly the same subset of variables. An example of a GRM form would be $x_1 x_2 x_3 \oplus \bar{x}_1 x_2 \oplus \bar{x}_2 x_3$, but the expression $x_2 x_3 \oplus \bar{x}_1 x_2 \oplus \bar{x}_2 x_3$ would not be a GRM because the terms $x_2 x_3$ and $\bar{x}_2 x_3$ both have the subset of variables $\{x_2, x_3\}$. A GRM form is formally defined in Definition 3.

Definition 3. A binary Generalized Reed-Muller (GRM) form of a single-output function $f(x_1, x_2, \dots, x_n)$ is the function in the form of Eq. (3), where \hat{x}_i can be either positive polarity (x_i) or negative polarity (\bar{x}_i), and $a_i \in \{0, 1\}$.

$$f(x_1, x_2, \dots, x_n) = a_0 \oplus a_1(\hat{x}_1) \oplus a_2(\hat{x}_2) \oplus \dots \oplus a_{2^n-1}(\hat{x}_1 \hat{x}_2 \dots \hat{x}_n) \quad (3)$$

□

A function of n variables has one PPRM form, 2^n possible FPRM forms, and $2^{n2^{n-1}}$ possible GRM forms. In this paper, we generalize these forms to multi-valued input logic in Section 3.5 and utilize them for quantum circuit synthesis.

2.2 Boolean Expansions

This section presents the *Shannon expansion* [26], *positive Davio expansion* [27], and *negative Davio expansion* [27].

The XOR version of the Shannon expansion is expressed in Eq. (4), where the cofactor $f_{\bar{a}}$ is the function f with $a = 0$, and the cofactor f_a is the function f with $a = 1$.

$$f = \bar{a} f_{\bar{a}} \oplus a f_a \quad (4)$$

The positive and negative Davio expansions can be derived from the Shannon expansion. The positive Davio expansion, stated in Eq. (5), can be found by substituting $\bar{a} = 1 \oplus a$.

$$\begin{aligned} f &= \bar{a} f_{\bar{a}} \oplus a f_a \\ &= (1 \oplus a) f_{\bar{a}} \oplus a f_a \\ &= f_{\bar{a}} \oplus a f_{\bar{a}} \oplus a f_a \\ &= f_{\bar{a}} \oplus a(f_{\bar{a}} \oplus f_a) \end{aligned} \quad (5)$$

Similarly, the negative Davio expansion, stated in Eq. (6), can be found by substituting $a = 1 \oplus \bar{a}$.

$$\begin{aligned}
f &= \bar{a}f_{\bar{a}} \oplus af_a \\
&= \bar{a}f_{\bar{a}} \oplus (1 \oplus \bar{a})f_a \\
&= \bar{a}f_{\bar{a}} \oplus f_a \oplus \bar{a}f_a \\
&= f_a \oplus \bar{a}(f_{\bar{a}} \oplus f_a)
\end{aligned} \tag{6}$$

These expansions are generalized to ternary input logic in Section 3.4.

2.3 Reversible Quantum Gates

This section presents the gates that we use to synthesize circuits from Exclusive-or Sum of Products (ESOP) expressions or RM forms: the quantum *NOT gate*, *Controlled-NOT (CNOT) gate*, and *n-bit Toffoli gate*, which are shown in Fig. 1a, Fig. 1b, and Fig. 1d, respectively. The NOT gate acts as the NOT operation, the CNOT gate acts as the XOR operation, and the *n*-bit Toffoli gate acts as both an AND operation and an XOR operation. These gates will appear in circuits throughout this paper. Minimizing the number of inputs to the Toffoli gates in a circuit is a current problem that many researchers face, which heavily impacts the quantum cost, as discussed in the next subsection.

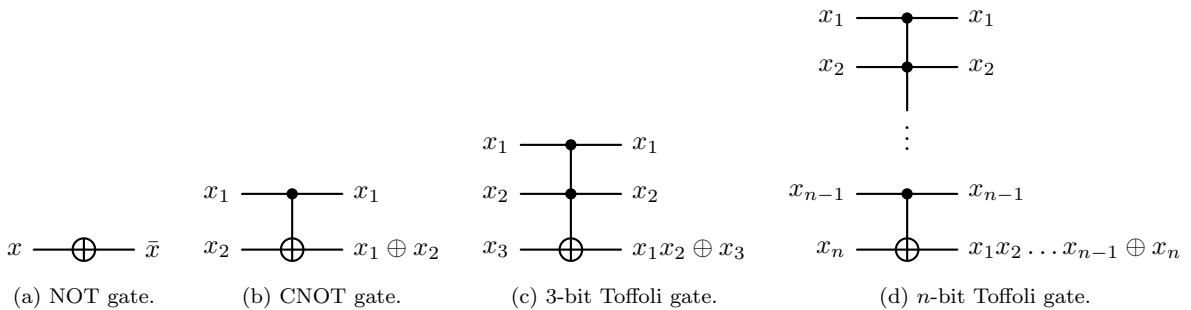


Figure 1: Reversible quantum gates.

2.4 Quantum Costs

The cost of a circuit can be calculated in many ways, two of which are the Maslov cost [15] and the Transpilation Quantum Cost (TQC) [16, 17].

The Maslov cost is a metric that sums up the individual cost of all the different Toffoli gates depending on the number of controls, with zero controls being equivalent to a NOT gate, one control being equivalent to a CNOT gate, and two controls being equivalent to a standard 3-bit Toffoli gate, with the Maslov cost for these gates listed in Table 1.

The Transpilation Quantum Cost (TQC) is a metric that calculates the quantum cost of a circuit after transpilation. This cost was originally designed for IBM QPUs, but it can be used for any hardware. The TQC of a circuit is determined by Eq. (7), where N_1 is the number of native single-qubit gates, N_2 is the number of native double-qubit gates, XC is the number of SWAP gates, and D is the depth.

$$TQC = N_1 + N_2 + XC + D \tag{7}$$

The general quantum costs for different gates are stated in Table 1. The Maslov cost directly calculates the final cost of a function's cost-expensive circuit realization, so it is a technology-independent approach. However, the TQC calculates the cost of the final transpiled circuit and is a technology-dependent approach. The TQC in this paper is calculated based on the IBM Torino quantum computer [28].

Note that the cost of Toffoli gates with many inputs increases almost exponentially with each input qubit added.

Gate	Maslov Cost	TQC
NOT	1	1
CNOT	1	14
3-Bit Toffoli	5	54
4-Bit Toffoli	13	109
5-Bit Toffoli	29	219

Table 1: Quantum cost of different reversible gates.

2.5 ESOP versus GRM and Factorization

This subsection presents an example that illustrates the difference between realizing a circuit from a non-GRM ESOP expression, a GRM, and a factorized GRM.

Example 1. Let $f = x_1x_2x_3 \oplus \bar{x}_1\bar{x}_2\bar{x}_3$, where x_1 , x_2 , and x_3 are binary variables.

If the reversible quantum circuit was realized directly from the ESOP expression, then that would lead to the circuit in Fig. 2a, which contains 3 NOT gates and 2 4-bit Toffoli gates. Thus, the circuit has a Maslov cost of 29 and a TQC of 221.

However, f is equal to the GRM form $x_1x_2 \oplus \bar{x}_1\bar{x}_3 \oplus x_2\bar{x}_3$, as shown on the Karnaugh map in Fig. 3. The circuit realization of this GRM is illustrated in Fig. 2b. This circuit consists of 2 NOT gates and 3 3-bit Toffoli gates, and thus has a Maslov cost of 17 and a TQC of 164, which is less costly compared to the non-GRM ESOP. Even though the GRM form has more terms, the terms each have fewer literals, decreasing the number of inputs to the Toffoli gates.

The cost of the circuit can be further minimized by factoring the GRM form for f to $x_1x_2 \oplus (\bar{x}_1 \oplus x_2)\bar{x}_3$. The circuit realization, shown in Fig. 2c, consists of 2 NOT gates, 1 CNOT gate, and 2 3-bit Toffoli gates, and thus has a Maslov cost of 13 and a TQC of 124, making it less costly than both the non-GRM ESOP and the GRM.

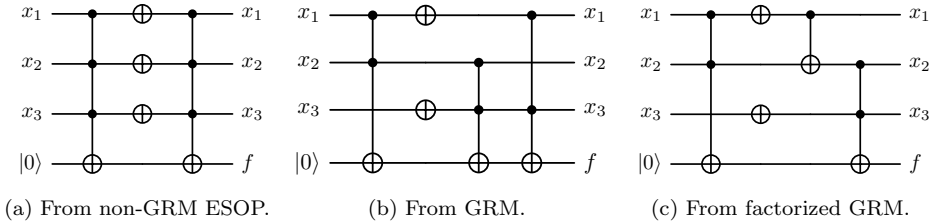


Figure 2: Reversible quantum circuit realizations of f from Example 1.

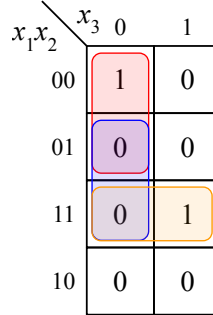


Figure 3: Karnaugh map of f showing the groups for the GRM form: $x_1x_2 \oplus \bar{x}_1\bar{x}_3 \oplus x_2\bar{x}_3$.

Aiming for GRM forms and factorizing expressions to reduce the number of literals in a product and thus the number of inputs to the Toffoli gates is a core part of our methodology to minimize circuits.

2.6 Butterfly Diagrams

There are many fundamentally different concepts of a “butterfly diagram” in physics, astronomy [29], computer engineering, systems theory, and other fields. The concept of *butterfly diagram* used in engineering is different than those in other areas, and it is useful for mathematical structure, visualization of algorithms, and efficient realization in parallel hardware. Well-known butterfly diagrams are created for the Fourier [30–32], Haar [33], Hadamard [33], and other spectral transforms. Less popular are diagrams created for Fixed-Polarity Reed-Muller transforms [34, 35]. In this paper, we create new classes of butterfly diagrams that are useful to synthesize ternary input quantum circuits and binary quantum circuits with decoders.

Examples of butterfly diagram kernels are shown in Fig. 4a, Fig. 4b, and Fig. 4c, which correspond to the Shannon, positive Davio, and negative Davio expansions, respectively. In Fig. 4, the red variables represent the inputs, while the blue variables represent the values the inputs are multiplied by. The middle part is the butterfly diagram kernel, where the points where the lines meet represent an XOR operation, and both sides correspond to the same function.

For these butterfly diagrams, the left side represents the Shannon expansion, $f = \bar{a}f_{\bar{a}} \oplus af_a$, where the inputs are the cofactors. The right side represents their respective expansions, which are stated in the respective captions.

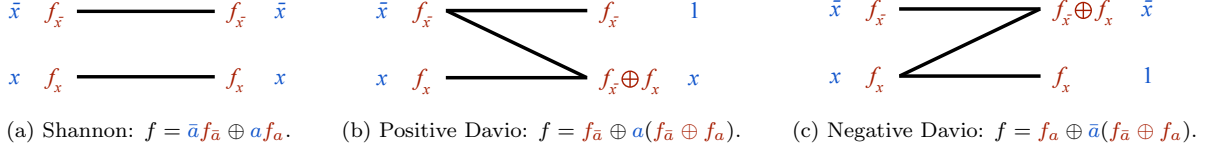


Figure 4: The butterfly diagram kernels for the binary Shannon, positive Davio, and negative Davio expansions.

The positive Davio expansion also represents converting the variable a to positive polarity, and the negative Davio expansion represents converting the variable a to negative polarity. Applying this method for each variable in a function can be used to transform a function from its *minterms* to an FPRM, where the minterms are the terms that contain literals for all variables.

An example of a butterfly diagram for a two-variable function which converts minterms to an FPRM of polarity 01 (x_1 is negative polarity and x_2 is positive polarity) is shown in Fig. 5. The first layer (column) of the butterfly diagram converts all instances of the variable x_2 to positive polarity with the positive Davio butterfly diagram kernels, and the second layer converts all instances of the variable x_1 to negative polarity with the negative Davio butterfly diagram kernels. The inputs and outputs for the function $\bar{x}_1\bar{x}_2 \oplus x_1\bar{x}_2 \oplus x_1x_2$, which has the FPRM form $\bar{x}_1x_2 \oplus 1$ are listed in the figure. A value of 1 means that the corresponding term is in the function, while a value of 0 means that it is not. The concept of butterfly diagrams for FPRM forms is expanded to multi-valued input logic in Section 7.

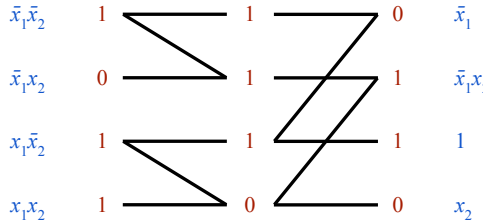


Figure 5: The butterfly diagram that transforms a function of x_1 and x_2 from the XOR of minterms: $\bar{x}_1\bar{x}_2 \oplus x_1\bar{x}_2 \oplus x_1x_2$, to the FPRM form with polarity 01: $\bar{x}_1x_2 \oplus 1$.

3 Multi-Valued Input, Binary Output Functions

In literature [36], the concept of multi-valued input, multi-valued output functions related to the classical Reed-Muller (RM) forms exists. However, this paper introduces a new structural design for binary quantum circuits based on canonical forms, namely MVI-FPRM and MVI-GRM, for *multi-valued input, binary output* (MVI) functions. In general [2–9], quantum circuits are synthesized from ESOP [25, 37–42] expressions (also known as AND-XOR expressions, Boolean polynomials, or Zhegalkin polynomials) that are formally built with two levels, or similar circuits. In contrast, the circuit structure from this paper has three levels: a decoder level, an AND level, and an XOR level. Because MVI functions use multi-valued variables as a representation of multiple binary variables, MVI functions are realized as binary circuits rather than multi-valued circuits. Our goal is to avoid large, expensive n -bit Toffoli gates ($n > 3$). Circuits from these MVI functions can then be used to construct blocks such as logical comparators and arithmetic circuits, in the oracles of different quantum search algorithms, such as Grover’s Algorithm [43], BHT-QAOA [44], and the Quantum Walk Algorithm [45].

In addition, our defined forms and related optimization methods can be used in the future, when ternary input, binary output technology [36] becomes available for quantum reversible circuits.

In this paper, binary variables will be denoted by lowercase letters (x) and multi-valued variables will be denoted by uppercase letters (X).

Definition 4. A multi-valued input, completely specified binary output (MVI) function is a mapping $F(X_1, X_2, \dots, X_n) : V_1 \times V_2 \times \dots \times V_n \rightarrow \{0, 1\}$, where X_i is a multi-valued variable that takes in a value from the set $V_i = \{0, 1, \dots, v_i - 1\}$, where v_i is the radix. \square

It is important to note that MVI functions can take in variables of any *radix*, meaning that the variables could be ternary (3-valued), quaternary (4-valued), quinary (5-valued), or another radix. The variables for an MVI function are also not required to be of the same radix. For example, a function could take in the quaternary variable X_1 and the ternary variable X_2 .

In binary logic, a literal is equal to 1 if $x = 1$, and it is positive (x) polarity, or if $x = 0$, and it is negative (\bar{x}) polarity. Extending this to MVI logic leads to the definition of a *multi-valued input (MVI) literal* in Definition 5.

Definition 5. A multi-valued input, binary output (MVI) literal of the multi-valued variable X for a given set of truth values $S \subseteq V = \{0, 1, \dots, v-1\}$, denoted by X^S , is defined as

$$X^S = \begin{cases} 1 & \text{if } X \in S \\ 0 & \text{if } X \notin S. \end{cases}$$

□

For instance, the literal $X^{1,2,3}$ is equal to 1 if the variable X is equal to 1, 2, or 3. Otherwise, the literal is equal to 0. The variable X , which is inputted, is multi-valued. However, the literal $X^{1,2,3}$, which is outputted, is binary. A product of literals ($X_1^{S_1} X_2^{S_2} \dots X_n^{S_n}$) is a *product term*, which is also called a *product* or *term* for short, and is also a binary value. An MVI literal with a single value (only one element in S , e.g., X^0 and X^2) will be called a *single-valued literal*. One method of realizing an MVI function as a binary quantum circuit is demonstrated in Example 2.

Example 2. The goal is to create a circuit for the function $f = X_1^{0,2,3} X_2^{0,1}$, where X_1 and X_2 are quaternary (4-valued) variables.

x_{1a}	x_{1b}	X_1	x_{2a}	x_{2b}	X_2
0	0	0	0	0	0
0	1	1	0	1	1
1	0	2	1	0	2
1	1	3	1	1	3

(a) X_1 in terms of the binary variables x_{1a} and x_{1b} . (b) X_2 in terms of the binary variables x_{2a} and x_{2b} .

Table 2: X_1 and X_2 encoded by binary variables.

To create a binary circuit for this function, we can represent the quaternary variables X_1 and X_2 with the binary variables x_{1a} and x_{1b} for X_1 , and x_{2a} and x_{2b} for X_2 . As shown in Table 2, the value for 0 can be encoded as 00, 1 as 01, 2 as 10, and 3 as 11. Converting the tables into Karnaugh maps for X_1 and X_2 in terms of x_{1a}, x_{1b}, x_{2a} , and x_{2b} gives the maps shown in Fig. 6. Karnaugh maps for the literals in the function f , $X_1^{0,2,3}$ and $X_2^{0,1}$, are also shown in Fig. 6.

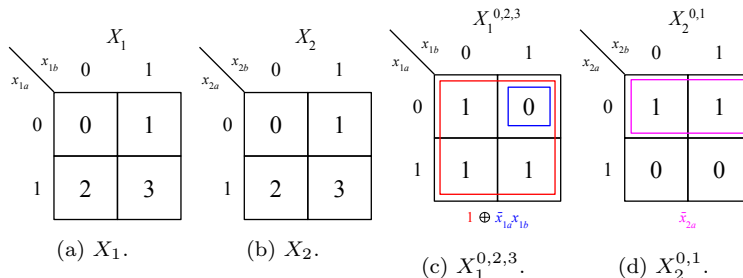


Figure 6: Karnaugh maps for X_1 , X_2 and the literals $X_1^{0,2,3}$, $X_2^{0,1}$ encoded by binary variables for Example 2.

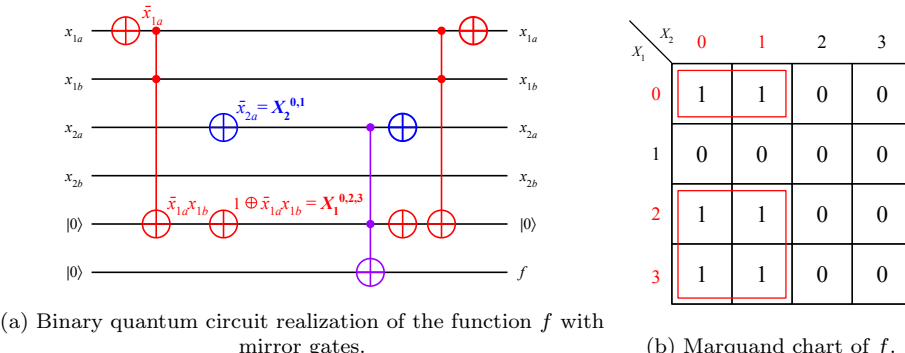


Figure 7: The circuit and Marquand chart of $f = X_1^{0,2,3} X_2^{0,1}$ for Example 2.

From the groupings shown in Fig. 6 for $X_1^{0,2,3}$, it can be found that $X_1^{0,2,3} = 1 \oplus \bar{x}_{1a}x_{1b}$ and $X_2^{0,1} = \bar{x}_{2a}$. f can be realized as the circuit shown in Fig. 7a. This function is also represented in the Marquand chart shown in Fig. 7b. The rows represent the possible values of X_1 and the columns represent the possible values of X_2 . The numbers in the cells represent the value of f for the given values of X_1 and X_2 . The values of X_1 and X_2 that lead to a value of 1 for their respective literals $X_1^{0,2,3}$ and $X_2^{0,1}$ are in red. Note that the function f is only equal to 1 if both literals are 1, and that the MVI expression naturally factorizes the function. Also note that the values listed for the rows and columns of the Marquand chart are in natural order, and that, in contrast to Karnaugh maps, the groupings on the Marquand chart are not required to be adjacent.

3.1 Operating with Multi-Valued Input Literals

Many laws of Boolean algebra [46, 47] can be extended to MVI literals. This section covers the basic operations for algebraically manipulating equations dealing with these literals.

Notably, X^S is always 1 when $S = V = \{0, 1, \dots, v-1\}$, so $X^V = 1$, and X^S is always 0 when $S = \emptyset$, where \emptyset is the empty set, and X is a v -valued variable ($v \geq 2$). The AND, OR, and XOR operations ($X_1^{S_1}X_2^{S_2}$, $X_1^{S_1} + X_2^{S_2}$, and $X_1^{S_1} \oplus X_2^{S_2}$) are identical to Boolean algebra, since the literals are binary. However, when applying the AND, OR, and XOR operations on literals of the same variable, e.g., $X^{1,2} \oplus X^{0,1}$, there are rules to simplify such expressions, as stated in Eq. (8), Eq. (9), and Eq. (10) respectively, where \cup is set union, \cap is set intersection, and Δ is set symmetric difference. The symmetric difference $A\Delta B$ of two sets A and B is equal to the set of all elements in either A or B but not both, as the set counterpart to the XOR operation.

$$X^{S_1}X^{S_2} = X^{S_1 \cap S_2} \quad (8)$$

$$X^{S_1} + X^{S_2} = X^{S_1 \cup S_2} \quad (9)$$

$$X^{S_1} \oplus X^{S_2} = X^{S_1 \Delta S_2} \quad (10)$$

$$\overline{X^S} = 1 \oplus X^S = X^{V \Delta S} \quad (11)$$

For example, $X^{0,1,3,4}X^{1,2,4} = X^{1,4}$, $X^{0,1,3,4} + X^{1,2,4} = X^{0,1,2,3,4}$, and $X^{0,1,3,4} \oplus X^{1,2,4} = X^{0,2,3}$.

The NOT operation in Boolean ring algebra is $\bar{x} = 1 \oplus x$. The NOT operation for MVI logic is similarly defined in Eq. (11). For example, for the quinary (5-valued) variable X , $\overline{X^{0,1,4}} = X^{2,3}$.

In this paper, the AND and XOR operations will be utilized, where the AND operation can be realized with a Toffoli gate, and the XOR operation can be realized with a CNOT or Toffoli gate.

3.2 Decoders

A decoder converts binary variables into MVI literals. All possible literals should be able to be represented by an XOR expression of the decoder's outputted literals, as shown in Example 3.

Example 3. Let X be a ternary (3-valued) variable, which is encoded by the binary variables x_1 and x_2 . A possible decoder for X can output the literals $X^{1,2}$, X^1 , and X^0 . Every literal can be created by an XOR expression with the outputted literals, as shown in Table 3. Any literals of X that are needed can then be synthesized using CNOT gates.

Literal	Binary Code	In Terms of the Outputted Literals
X^2	001	$X^{1,2} \oplus X^1$
X^1	010	X^1
$X^{1,2}$	011	$X^{1,2}$
X^0	100	X^0
$X^{0,2}$	101	$X^{1,2} \oplus X^1 \oplus X^0$
$X^{0,1}$	110	$X^1 \oplus X^0$
$X^{0,1,2}$	111	$X^{1,2} \oplus X^0$

Table 3: All literals represented by a binary code and XOR expression with $X^{1,2}$, X^1 , and X^0 for Example 3.

This decoder can also be represented as the *polarity matrix* P .

$$P = \begin{bmatrix} 0 & 1 & 2 \\ 0 & 1 & 1 \\ 0 & 1 & 0 \\ 1 & 0 & 0 \end{bmatrix} = \begin{bmatrix} T^1 \\ T^2 \\ T^3 \end{bmatrix}$$

The first row represents the literal $X^{1,2}$, since the values in column 1 and column 2 are 1, where the columns are labeled with the first column as 0. The second row represents the literal X^1 , since the value of column 1 is 1. And the third row represents the literal X^0 , since the value of column 0 is 1.

The rows, which correspond to each outputted literal, can be represented as the row vectors T^1 , T^2 , and T^3 . Note that these vectors are *linearly independent*, meaning that no vector in the set T^1 , T^2 , T^3 can be obtained from linearly operating on the other vectors [48]. Here, XOR is the linear operation used. The polarity matrix P , or more generally P_i , will be elaborated on in the next subsection.

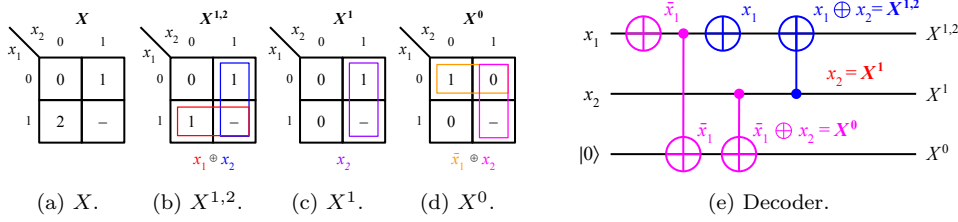


Figure 8: Karnaugh maps and the decoder for the literals $X^{1,2}$, X^1 , and X^0 in Example 3.

The realization of a binary quantum circuit for this decoder is shown in Fig. 8e.

3.3 Polarity With Multi-Valued Input Literals

In binary logic, the polarity is either negative or positive. However, for v -valued logic, the polarity is defined as a matrix since all possible functions can only be defined with at least v different literals. The literals represented by the polarity matrix P from Example 3 correspond to the decoder's outputted literals. The polarity matrix is formally defined in Definition 6.

Definition 6. The polarity matrix P (or polarity for short) of a multi-valued variable X is a matrix where the r th row vector T^r of the matrix is the binary representation of the polarity literal P^r . \square

The concept of polarity for multi-valued variables is formally expanded on in Theorem 1.

Theorem 1. A multi-valued literal X^S , where $S \subseteq V = \{0, 1, \dots, v-1\}$, can be represented by v polarity literals P^1, P^2, \dots, P^v . The values of the polarity literals form the row vectors T^r of the linearly independent $v \times v$ matrix P .

Proof. A property of a linearly independent $m \times m$ matrix O ($m \in \mathbb{N}$) with elements $o_{ij} \in \{0, 1\}$ is that any m -dimensional vector U with elements $u_{ij} \in \{0, 1\}$ can be represented as a bit-by-bit XOR operation on the row vectors of the matrix O .

Thus, any set of truth values $S \subseteq V = \{0, 1, \dots, v-1\}$ of a literal X^S can be represented as an XOR expression of the values P^r with $r \subseteq V = \{0, 1, \dots, v-1\}$, where T^r is the r th row vector of the linearly independent $v \times v$ matrix P . \square

Theorem 1 states that any MVI literal X^S can be expressed in terms of the polarity literals of a polarity P . Note that a form, according to Theorem 1, is a canonical form, meaning that the form is unique for each function and polarity. This is because the polarity matrix P is linearly independent.

The number of potential polarities n_P (where order does not matter) for an v -valued variable is stated in Eq. 12 [48].

$$n_P = \frac{1}{v!} \prod_{k=0}^{v-1} 2^v - 2^k \quad (12)$$

The number of polarities from binary (2-valued) to quinary (5-valued) logic is shown in Table 4.

	Number of Polarities
Binary (2-Valued)	3
Ternary (3-Valued)	28
Quaternary (4-Valued)	840
Quinary (5-Valued)	83,328

Table 4: Number of polarities for different valued logic.

All 28 of the possible polarities for a ternary (3-valued) variable are listed in Table 5

Vectors that are not linearly independent can also be used to represent the polarity literals. Thus, Theorem 1 can be generalized to Lemma 1.

$\begin{bmatrix} 1 & 0 & 0 \\ 0 & 1 & 0 \\ 0 & 0 & 1 \end{bmatrix}$	$\begin{bmatrix} 1 & 0 & 0 \\ 0 & 1 & 0 \\ 1 & 0 & 1 \end{bmatrix}$	$\begin{bmatrix} 1 & 0 & 0 \\ 0 & 1 & 0 \\ 0 & 1 & 1 \end{bmatrix}$	$\begin{bmatrix} 1 & 0 & 0 \\ 0 & 1 & 0 \\ 1 & 1 & 1 \end{bmatrix}$	$\begin{bmatrix} 1 & 0 & 0 \\ 0 & 0 & 1 \\ 1 & 1 & 0 \end{bmatrix}$	$\begin{bmatrix} 1 & 0 & 0 \\ 0 & 0 & 1 \\ 0 & 1 & 0 \end{bmatrix}$	$\begin{bmatrix} 1 & 0 & 0 \\ 0 & 0 & 1 \\ 0 & 1 & 1 \end{bmatrix}$	$\begin{bmatrix} 1 & 0 & 0 \\ 0 & 0 & 1 \\ 1 & 1 & 1 \end{bmatrix}$
$\begin{bmatrix} 1 & 0 & 0 \\ 1 & 0 & 0 \\ 1 & 0 & 1 \end{bmatrix}$	$\begin{bmatrix} 1 & 0 & 0 \\ 1 & 1 & 0 \\ 0 & 1 & 1 \end{bmatrix}$	$\begin{bmatrix} 1 & 0 & 0 \\ 1 & 1 & 0 \\ 1 & 1 & 1 \end{bmatrix}$	$\begin{bmatrix} 1 & 0 & 0 \\ 1 & 0 & 1 \\ 0 & 1 & 1 \end{bmatrix}$	$\begin{bmatrix} 1 & 0 & 0 \\ 1 & 0 & 1 \\ 1 & 1 & 1 \end{bmatrix}$	$\begin{bmatrix} 0 & 1 & 0 \\ 0 & 0 & 1 \\ 1 & 1 & 0 \end{bmatrix}$	$\begin{bmatrix} 0 & 1 & 0 \\ 0 & 0 & 1 \\ 1 & 0 & 1 \end{bmatrix}$	$\begin{bmatrix} 0 & 1 & 0 \\ 0 & 0 & 1 \\ 1 & 0 & 1 \end{bmatrix}$
$\begin{bmatrix} 0 & 1 & 0 \\ 0 & 0 & 1 \\ 1 & 1 & 1 \end{bmatrix}$	$\begin{bmatrix} 0 & 1 & 0 \\ 1 & 1 & 0 \\ 1 & 0 & 1 \end{bmatrix}$	$\begin{bmatrix} 0 & 1 & 0 \\ 1 & 1 & 0 \\ 0 & 1 & 1 \end{bmatrix}$	$\begin{bmatrix} 0 & 1 & 0 \\ 1 & 1 & 0 \\ 1 & 1 & 1 \end{bmatrix}$	$\begin{bmatrix} 0 & 1 & 0 \\ 1 & 0 & 1 \\ 0 & 1 & 1 \end{bmatrix}$	$\begin{bmatrix} 0 & 1 & 0 \\ 0 & 1 & 1 \\ 1 & 1 & 1 \end{bmatrix}$	$\begin{bmatrix} 0 & 1 & 0 \\ 0 & 1 & 1 \\ 1 & 0 & 1 \end{bmatrix}$	$\begin{bmatrix} 0 & 0 & 1 \\ 1 & 1 & 0 \\ 1 & 0 & 1 \end{bmatrix}$
$\begin{bmatrix} 0 & 0 & 1 \\ 1 & 1 & 0 \\ 0 & 1 & 1 \end{bmatrix}$	$\begin{bmatrix} 0 & 0 & 1 \\ 1 & 0 & 1 \\ 0 & 1 & 1 \end{bmatrix}$	$\begin{bmatrix} 0 & 0 & 1 \\ 1 & 0 & 1 \\ 1 & 1 & 1 \end{bmatrix}$	$\begin{bmatrix} 0 & 0 & 1 \\ 0 & 1 & 1 \\ 1 & 1 & 1 \end{bmatrix}$	$\begin{bmatrix} 1 & 1 & 0 \\ 1 & 0 & 1 \\ 1 & 1 & 1 \end{bmatrix}$	$\begin{bmatrix} 1 & 1 & 0 \\ 0 & 1 & 1 \\ 1 & 1 & 1 \end{bmatrix}$	$\begin{bmatrix} 1 & 1 & 0 \\ 0 & 1 & 1 \\ 1 & 1 & 1 \end{bmatrix}$	$\begin{bmatrix} 1 & 0 & 1 \\ 0 & 1 & 1 \\ 1 & 1 & 1 \end{bmatrix}$

Table 5: All ternary polarities.

Lemma 1. Any set of vectors T^r can be used for the polarity literals P^r , if every possible set $S \subseteq V$ for the literal X^S can be generated by an AND-XOR expression with a subset of the polarity literals \square

In a polarity matrix P that is not linearly independent, there is more than one way to generate X^S from the given polarity literals. This is because, since P is not linearly independent, some vectors T^r (corresponding to P^r) can be represented by an XOR combination of other row vectors in P , leading to multiple representations of the same function. Thus, the XOR expressions created with such polarity literals are no longer canonical forms. These polarities can be used to make quantum circuits, but they are costlier than their linear independent alternatives.

Name	Symbol
Binary Variable	x
MVI Variable	X
MVI Literal	X^S
Set of Truth Values	S
Set of All Possible Truth Values	$V = \{0, 1, \dots, v - 1\}$
Polarity Matrix	P
Polarity Literal	P^r
Row Vector from Literal	T^r

Table 6: Notation.

Table 6 summarizes the notation used throughout this paper, although slight differences may appear (e.g., both P and Q will be used for polarity). When working with more than one variable, subscripts will be used, such as with $X_i^{S_i}$.

3.4 Ternary Input Shannon and Davio-like Expansions

The Shannon expansion [26], which is stated in Eq. (4), and the Davio expansions [27], which are stated in Eq. (5) and Eq. (6), from binary logic can be generalized to MVI logic. This subsection introduces similar expressions for ternary input logic.

Recall that the original Shannon expansion, with XOR, from Eq. (4) is

$$f = a f_a \oplus \bar{a} f_{\bar{a}}.$$

The literal a is 1 if $a = 1$, and the literal \bar{a} is 1 if $a = 0$. Thus, let $a = a^1$ and $\bar{a} = a^0$, where a^k is 1 if $a = k$. The cofactors f_a and $f_{\bar{a}}$ can be rewritten as $f_{a=1}$ and $f_{a=0}$, with $f_{a=k}$ equal to the function f when $a = k$.

The Shannon expansion can thus be rewritten as

$$\begin{aligned} f &= a^1 f_{a=1} \oplus a^0 f_{a=0} \\ &= a^0 f_{a=0} \oplus a^1 f_{a=1}. \end{aligned}$$

This can be extended to ternary input functions. The binary variable a can be replaced by the multi-valued variable X . The ternary input Shannon expansion is expressed in Eq. (13).

$$f = X^0 f_{X=0} \oplus X^1 f_{X=1} \oplus X^2 f_{X=2} \quad (13)$$

The polarity matrix for the ternary variable X with $P^1 = X^0$, $P^2 = X^1$, and $P^3 = X^2$ is

$$\begin{bmatrix} 1 & 0 & 0 \\ 0 & 1 & 0 \\ 0 & 0 & 1 \end{bmatrix}$$

which is equivalent to finding a function in terms of X^0 , X^1 , and X^2 . This is the same as finding the Shannon expansion.

Like their binary counterparts, the ternary input Davio-like expansions can be obtained from the ternary input Shannon expansion. One potential Davio-like expansion is shown in Eq. (14), which corresponds to the polarity with literals $X^{0,1,2} = 1$, $X^{0,1}$, and $X^{1,2}$.

$$\begin{aligned} f &= X^0 f_{X=0} \oplus X^1 f_{X=1} \oplus X^2 f_{X=2} \\ &= (1 \oplus X^{1,2}) f_{X=0} \oplus (1 \oplus X^{0,1} \oplus X^{1,2}) f_{X=1} \oplus (1 \oplus X^{0,1}) f_{X=2} \\ &= f_{X=0} \oplus X^{1,2} f_{X=0} \oplus f_{X=1} \oplus X^{0,1} f_{X=1} \oplus X^{1,2} f_{X=1} \oplus f_{X=2} \oplus X^{0,1} f_{X=2} \\ &= f_{X=0} \oplus f_{X=1} \oplus f_{X=2} \oplus X^{0,1} f_{X=1} \oplus X^{0,1} f_{X=2} \oplus X^{1,2} f_{X=0} \oplus X^{1,2} f_{X=1} \\ &= (f_{X=0} \oplus f_{X=1} \oplus f_{X=2}) \oplus X^{0,1} (f_{X=1} \oplus f_{X=2}) \oplus X^{1,2} (f_{X=0} \oplus f_{X=1}) \end{aligned} \quad (14)$$

However, this is not the only possible ternary input Davio-like expansion. Another variant is shown in Eq. (15), which corresponds to the polarity X^0 , $X^{0,1}$, $X^{0,2}$.

$$\begin{aligned} f &= X^0 f_{X=0} \oplus X^1 f_{X=1} \oplus X^2 f_{X=2} \\ &= X^0 f_{X=0} \oplus (X^0 \oplus X^{0,1}) f_{X=1} \oplus (X^0 \oplus X^{0,2}) f_{X=2} \\ &= X^0 f_{X=0} \oplus X^0 f_{X=1} \oplus X^{0,1} f_{X=1} \oplus X^0 f_{X=2} \oplus X^{0,2} f_{X=2} \\ &= X^0 f_{X=0} \oplus X^0 f_{X=1} \oplus X^0 f_{X=2} \oplus X^{0,1} f_{X=1} \oplus X^{0,2} f_{X=2} \\ &= X^0 (f_{X=0} \oplus f_{X=1} \oplus f_{X=2}) \oplus X^{0,1} (f_{X=1}) \oplus X^{0,2} (f_{X=2}) \end{aligned} \quad (15)$$

The other polarity matrices correspond to all the possible Davio-like expansions, so there are 27 Davio-like expansions in total. These relations can also be generalized to any multi-valued input logic.

Although multi-valued input Shannon and Davio-like expansions won't be elaborated further in this paper, they are important, as they link the concept of polarity for multi-valued input logic with classical Boolean algebra.

3.5 Extending Reed-Muller Forms to Multi-Valued Input Functions

The approach presented in this paper for generating multi-valued input FPRM forms, defined in Definition 7, is similar to those from [24]. We propose calling multi-valued input FPRM forms "MVI-FPRM" forms instead. Similarly, we call multi-valued input GRM forms, defined in Definition 8, "MVI-GRM" forms.

Before MVI-FPRM forms are formally defined, let us consider a simple example of such forms in Example 4, which shows the algebraic derivation.

Example 4. Take the MVI function $F_1 = X_1^{0,2,3} X_2^{0,1}$ with quaternary (4-valued) variable X_1 and ternary (3-valued) variable X_2 . Note that this differs from the function f in Example 2 because X_2 is ternary for F_1 while it was quaternary for f .

Suppose that the function has the polarity P_1, P_2 .

$$P_1 = \begin{bmatrix} 1 & 1 & 1 & 1 \\ 0 & 1 & 0 & 1 \\ 0 & 0 & 1 & 1 \\ 0 & 1 & 1 & 1 \end{bmatrix} = \begin{bmatrix} T_1^1 \\ T_1^2 \\ T_1^3 \\ T_1^4 \end{bmatrix}, \quad P_2 = \begin{bmatrix} 1 & 1 & 1 \\ 1 & 0 & 0 \\ 0 & 0 & 1 \end{bmatrix} = \begin{bmatrix} T_2^1 \\ T_2^2 \\ T_2^3 \end{bmatrix}$$

This means that the polarity literals for X_1 are

$$P_1^1 = X_1^{0,1,2,3} = 1, \quad P_1^2 = X_1^{1,3}, \quad P_1^3 = X_1^{2,3}, \quad P_1^4 = X_1^{1,2,3}.$$

The polarity literals for X_2 are

$$P_2^1 = X_2^{0,1,2} = 1, \quad P_2^2 = X_2^0, \quad P_2^3 = X_2^2.$$

The literals $X_1^{0,2,3}$ and $X_2^{0,1}$ can be represented in terms of the polarity literals as follows:

$$\begin{aligned} X_1^{0,2,3} &= P_1^1 \oplus P_1^3 \oplus P_1^4 \\ &= X_1^{0,1,2,3} \oplus X_1^{2,3} \oplus X_1^{1,2,3} \\ X_2^{0,1} &= P_2^1 \oplus P_2^3 \\ &= X_2^{0,1,2} \oplus X_2^2. \end{aligned}$$

From substituting these values into the function F_1 , taking into account that $P_1^1 = P_2^1 = 1$, and expanding, we obtain the MVI-FPRM form for F_1 , as demonstrated below:

$$\begin{aligned}
F_1 &= X_1^{0,2,3} X_2^{0,1} \\
&= (P_1^1 \oplus P_1^3 \oplus P_1^4)(P_2^1 \oplus P_2^3) \\
&= (1 \oplus P_1^3 \oplus P_1^4)(1 \oplus P_2^3) \\
&= 1 \oplus P_1^3 \oplus P_1^4 \oplus P_2^3 \oplus P_1^3 P_2^3 \oplus P_1^4 P_2^3 \\
&= 1 \oplus X_1^{2,3} \oplus X_1^{1,2,3} \oplus X_2^2 \oplus X_1^{2,3} X_2^2 \oplus X_1^{1,2,3} X_2^2.
\end{aligned}$$

Definition 7 extends the concept of FPRM forms for Boolean functions to the concept of MVI-FPRM forms for MVI functions.

Definition 7. The MVI-FPRM form of a single-output MVI function $F(X_1, X_2, \dots, X_n)$ with polarity P_1, P_2, \dots, P_n is defined with the so-called spectral coefficients $M_{P_1^{r_1}, P_2^{r_2}, \dots, P_n^{r_n}}$ in Eq. (16). Similar to binary FPRM forms, MVI-FPRM forms assign each variable a fixed polarity.

$$F(X_1, X_2, \dots, X_n) = \bigoplus_{r_i \in V_i} M_{P_1^{r_1}, P_2^{r_2}, \dots, P_n^{r_n}} P_1^{r_1} P_2^{r_2} \cdots P_n^{r_n} \quad (16)$$

□

Please note that while in binary, for a function of n variables, there are 2^n possible FPRM forms, but in the case of ternary input functions, there are 28^n MVI-FPRM forms, which makes synthesis much more difficult and points to the importance of selecting good decoders.

Recall that the binary GRM is defined as a form where each product term has a different set of variables than every other term. Therefore, we extend this to the MVI-GRM form.

Definition 8. The MVI-GRM form of a single-output MVI function is defined as a form where every two product terms have a different set of multi-valued variables. □

For instance, $X_1^{0,1} X_2^{0,2,3} \oplus X_1^{0,2} X_2^1$ is not an MVI-GRM form because both terms have the set of variables $\{X_1, X_2\}$, but $X_1^{0,1} X_2^{0,2,3} \oplus X_1^{0,2} X_3^1$ is an MVI-GRM form.

Although the names "spectral" and "spectrum" will be used, no knowledge of spectral theory is necessary. The spectral coefficients are a format for representing the MVI-FPRM form of a function with 0's and 1's.

The polarity of an MVI-FPRM form is defined in Definition 9.

Definition 9. The polarity of an MVI-FPRM form is the vector of polarity matrices describing the polarity for each multi-valued literal. □

4 Circuit Synthesis Based on MVI-FPRM

An approach for visualizing the MVI-FPRM form of a function using Marquand charts is shown in Example 5.

Example 5. The MVI-FPRM form of the function $F_1 = X_1^{0,2,3} X_2^{0,1}$ from Example 4 with polarities P_1 and P_2 can be represented by its spectrum M as shown in Fig. 9, which illustrates the standard trivial functions, which are all the possible product terms with the given polarity literals.

The function F_1 can be shown to be equal to

$$F_1 = 1 \oplus P_1^3 \oplus P_1^4 \oplus P_2^3 \oplus P_1^3 P_2^3 \oplus P_1^4 P_2^3$$

(remember that $P_1^1 = P_2^1 = 1$).

The MVI-FPRM form for this function can be visually verified by taking the XOR of the Marquand charts for each term in $1 \oplus P_1^3 \oplus P_1^4 \oplus P_2^3 \oplus P_1^3 P_2^3 \oplus P_1^4 P_2^3$ and comparing it to the Marquand chart for F_1 .

Let's start with the first two terms: 1 and P_1^3 . The first course of action is to draw both of the Marquand Charts for 1 and P_1^3 . Next, group together all the 1's in the Marquand charts, where the group for 1 is in red, while the group for P_1^3 is in blue. Then, overlap the two groups on a new Marquand chart. For each cell in the chart, if an odd number of groups cover it, then the value for that cell is 1; if an even number of groups cover it, then the value for that cell is 0. Fig. 10 shows the first step of the verification process, which combines all of the previous steps into one. The resulting Marquand chart is for the function $1 \oplus P_1^3$. This method essentially finds the XOR of the values in each cell for the functions, which is depicted in Fig. 11.

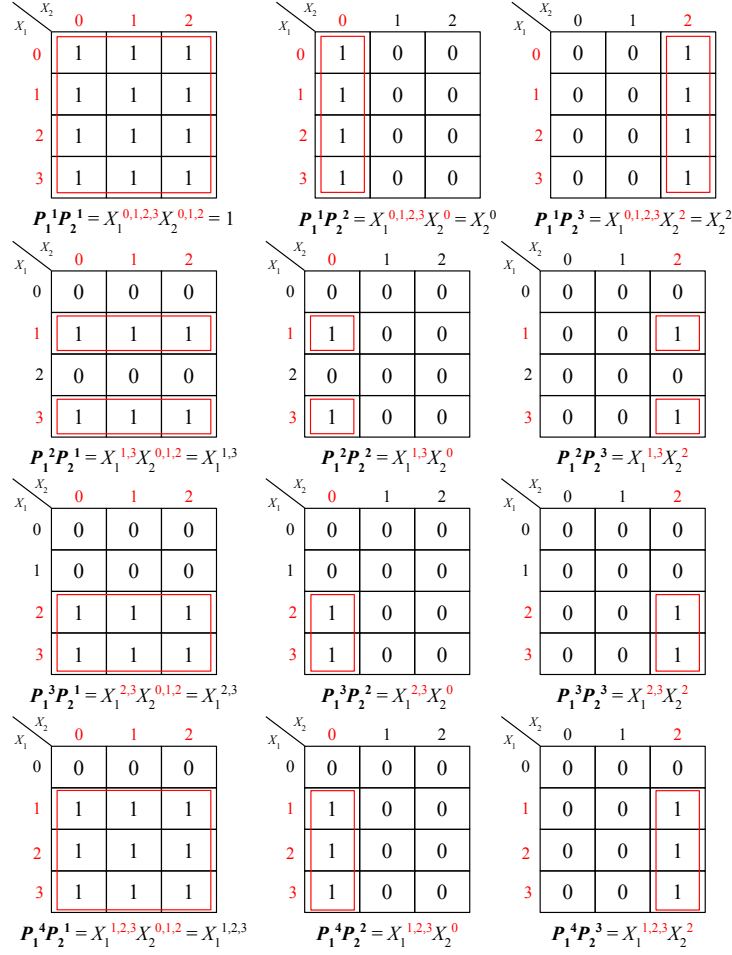


Figure 9: Standard trivial functions for variables X_1 and X_2 with polarities P_1 and P_2 respectively for Example 5.

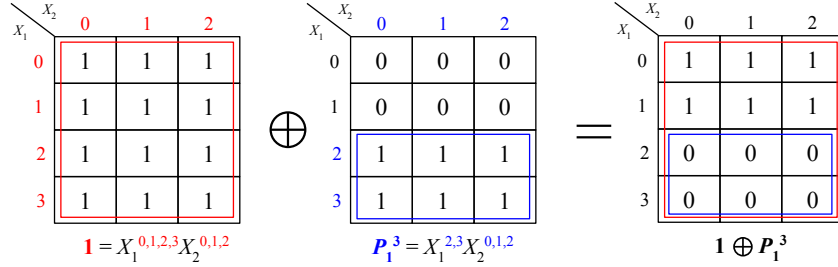


Figure 10: Step 1: XOR 1 and P_1^3 for Example 5.

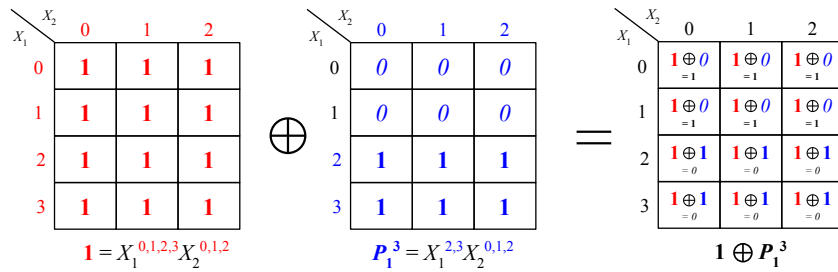
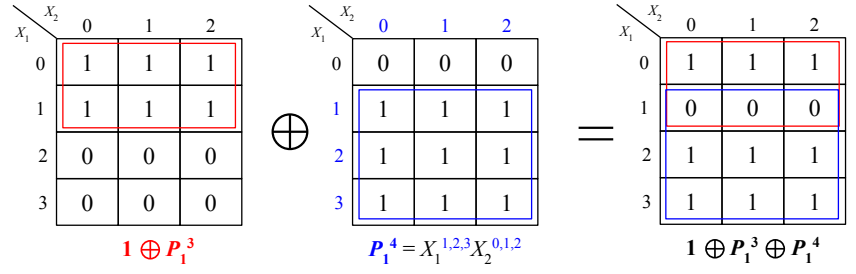


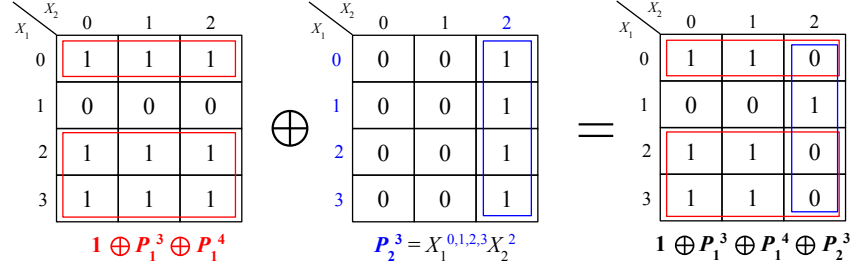
Figure 11: Process showing the XOR operation in each cell for Example 5.

Applying this strategy with all the other terms gives the Marquand charts shown in Fig. 12. The resulting chart is equal to the one in Fig. 13c, which is the Marquand chart that is obtained from the original function $F_1 = X_1^{0,2,3} X_2^{0,1}$.

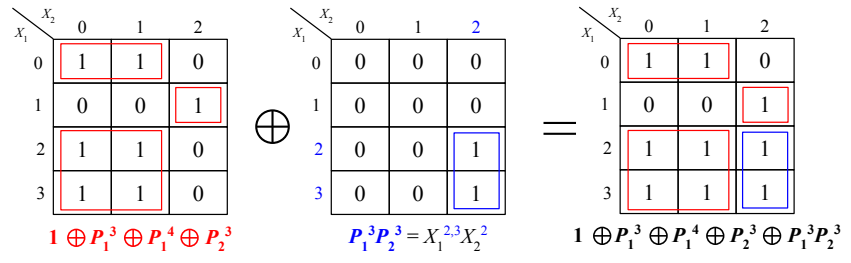
The spectral coefficients for the function F_1 with the polarities P_1 and P_2 are listed in Table 7. A value of 1 for the spectral coefficient $M_{P_1^{r_1} P_2^{r_2}}$ indicates that the corresponding term $P_1^{r_1} P_2^{r_2}$ is in the



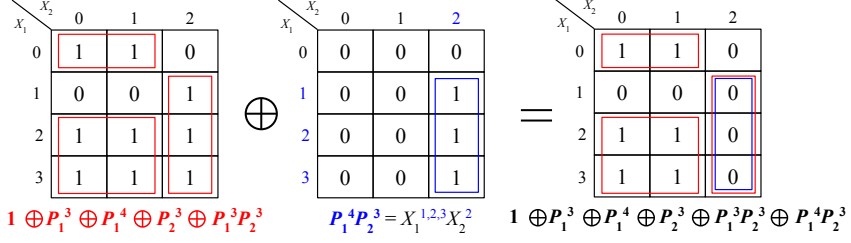
(a) Step 2: $1 \oplus P_1^3$ with P_1^4 .



(b) Step 3: $1 \oplus P_1^3 \oplus P_1^4$ with P_2^3 .



(c) Step 4: $1 \oplus P_1^3 \oplus P_1^4 \oplus P_2^3$ with $P_1^3 P_2^3$.



(d) Step 5: $1 \oplus P_1^3 \oplus P_1^4 \oplus P_2^3 \oplus P_1^3 P_2^3 \oplus P_1^4 P_2^3$ to get F_1 .

Figure 12: The remaining four steps for applying XOR on the Marquand charts for all terms in $1 \oplus P_1^3 \oplus P_1^4 \oplus P_2^3 \oplus P_1^3 P_2^3 \oplus P_1^4 P_2^3$ for Example 5.

MVI-FPRM form of the function F_1 , while a value of 0 indicates that it is not.

Coefficient	$M_{P_1^1 P_2^1}$	$M_{P_1^1 P_2^2}$	$M_{P_1^1 P_2^3}$	$M_{P_1^2 P_2^1}$	$M_{P_1^2 P_2^2}$	$M_{P_1^2 P_2^3}$	$M_{P_1^3 P_2^1}$	$M_{P_1^3 P_2^2}$	$M_{P_1^3 P_2^3}$	$M_{P_1^4 P_2^1}$	$M_{P_1^4 P_2^2}$	$M_{P_1^4 P_2^3}$
Value	1	0	1	0	0	0	1	0	1	1	0	1

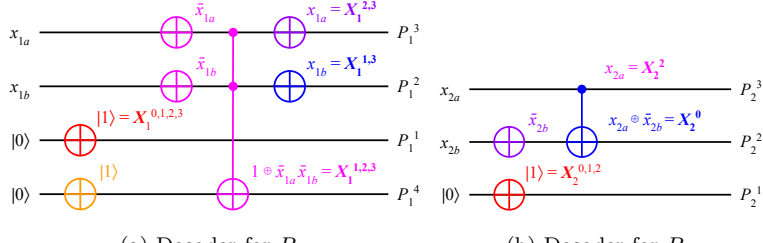
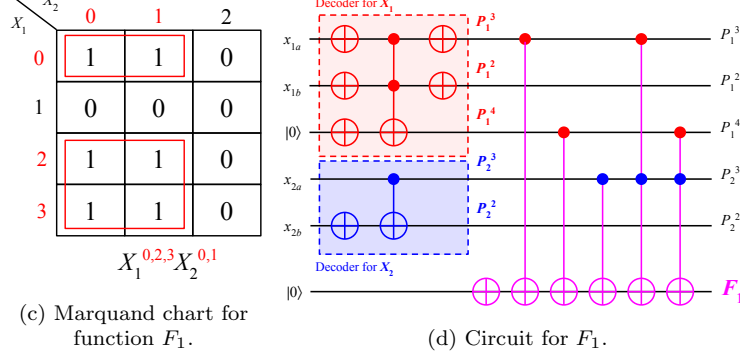
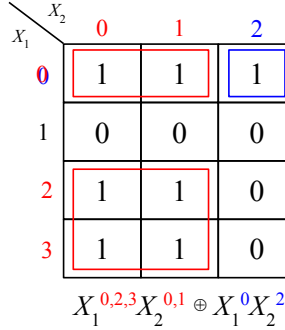
Table 7: Spectrum of function F_1 for Example 5.

Fig. 13a shows the decoder for P_1 (with X_1 encoded by binary variables x_{1a} and x_{1b}) and Fig. 13b shows the decoder for P_2 (with X_2 encoded by binary variables x_{2a} and x_{2b}). Realizing F_1 as a binary quantum circuit leads to the circuit shown in Fig. 13d, which uses the results of the decoders (with P_1^1 and P_2^1 omitted because they both equal 1) to calculate F_1 . It can be noted that the bigger the circuit is, the more negligible the cost of the decoders becomes.

So far, the examples have covered functions with only one product term. However, these methods can also apply to functions with multiple terms, as demonstrated in Example 6.

Example 6. The MVI-FPRM form of the function $F_2 = X_1^{0,2,3} X_2^{0,1} \oplus X_1^0 X_2^2$ with the same polarities from Examples 4 and 5 can be calculated by finding the XOR of the MVI-FPRM forms for the terms $X_1^{0,2,3} X_2^{0,1}$ and $X_1^0 X_2^2$.

The Marquand chart for F_2 is shown in Fig. 14.

(a) Decoder for P_1 .(b) Decoder for P_2 .(c) Marquand chart for function F_1 .(d) Circuit for F_1 .Figure 13: Marquand chart, decoders for P_1 and P_2 , and circuit for F_1 from Example 5.Figure 14: Marquand chart for function F_2 from Example 6.

In Examples 4 and 5, it was found and verified that the MVI-FPRM form of the first term (F_1) is

$$\begin{aligned} X_1^{0,2,3} X_2^{0,1} &= P_1^1 P_2^1 \oplus P_1^3 P_2^1 \oplus P_1^4 P_2^1 \oplus P_1^1 P_2^3 \oplus P_1^3 P_2^3 \oplus P_1^4 P_2^3 \\ &= 1 \oplus P_1^3 \oplus P_1^4 \oplus P_2^3 \oplus P_1^3 P_2^3 \oplus P_1^4 P_2^3. \end{aligned}$$

The MVI-FPRM form of the second term, $X_1^0 X_2^2$, in the function can be found to be

$$\begin{aligned} X_1^0 X_2^2 &= P_1^1 P_2^3 \oplus P_1^4 P_2^3 \\ &= P_2^3 \oplus P_1^4 P_2^3. \end{aligned}$$

This is verified algebraically as follows:

$$\begin{aligned} P_1^1 P_2^3 \oplus P_1^4 P_2^3 &= (P_1^1 \oplus P_1^4) P_2^3 \\ &= (X_1^{0,1,2,3} \oplus X_1^{1,2,3}) X_2^2 \\ &= X_1^0 X_2^2. \end{aligned}$$

The MVI-FPRM form for the whole function F_2 can be found by using spectral coefficients or algebraically. Both methods will be done in this example, starting with spectral coefficients.

The spectral coefficients for the terms $X_1^{0,2,3} X_2^{0,1}$ and $X_1^0 X_2^2$ are listed in Table 8.

Coefficient	$M_{P_1^1 P_2^1}$	$M_{P_1^1 P_2^2}$	$M_{P_1^1 P_2^3}$	$M_{P_1^2 P_2^1}$	$M_{P_1^2 P_2^2}$	$M_{P_1^2 P_2^3}$	$M_{P_1^3 P_2^1}$	$M_{P_1^3 P_2^2}$	$M_{P_1^3 P_2^3}$	$M_{P_1^4 P_2^1}$	$M_{P_1^4 P_2^2}$	$M_{P_1^4 P_2^3}$
Value for $X_1^{0,2,3} X_2^{0,1}$	1	0	1	0	0	0	1	0	1	1	0	1
Value for $X_1^0 X_2^2$	0	0	1	0	0	0	0	0	0	0	0	1

Table 8: Spectrum of the functions $X_1^{0,2,3} X_2^{0,1}$ and $X_1^0 X_2^2$ for Example 6.

The spectral coefficients for F_2 can be calculated using the spectral coefficients from its terms $X_1^{0,2,3}X_2^{0,1}$ and $X_1^0X_2^2$.

This process is expressed in Table 9, where the XOR of the spectral coefficients for $X_1^{0,2,3}X_2^{0,1}$ and $X_1^0X_2^2$ in each column is calculated, and the result is the spectral coefficient for F .

Coefficient	$M_{P_1^1 P_2^1}$	$M_{P_1^1 P_2^2}$	$M_{P_1^1 P_2^3}$	$M_{P_1^2 P_2^1}$	$M_{P_1^2 P_2^2}$	$M_{P_1^2 P_2^3}$	$M_{P_1^3 P_2^1}$	$M_{P_1^3 P_2^2}$	$M_{P_1^3 P_2^3}$	$M_{P_1^4 P_2^1}$	$M_{P_1^4 P_2^2}$	$M_{P_1^4 P_2^3}$
Value for $X_1^{0,2,3}X_2^{0,1}$	1	0	1	0	0	0	1	0	1	1	0	1
Value for $X_1^0X_2^2$	0	0	1	0	0	0	0	0	0	0	0	1
Value for F	1	0	0	0	0	0	1	0	1	1	0	0

Table 9: Spectrum of the function F_2 from Example 6.

From the resulting spectral coefficients, it can be found that

$$\begin{aligned} F_2 &= P_1^1 P_2^1 \oplus P_1^3 P_2^1 \oplus P_1^3 P_2^3 \oplus P_1^4 P_2^1 \\ &= 1 \oplus P_1^3 \oplus P_1^3 P_2^3 \oplus P_1^4 \\ &= 1 \oplus X_1^{2,3} \oplus X_1^{2,3} X_2^2 \oplus X_1^{1,2,3}. \end{aligned}$$

Calculating the MVI-FPRM form of F_2 algebraically yields the same results, as done below:

$$\begin{aligned} F_2 &= X_1^{0,2,3} X_2^{0,1} \oplus X_1^0 X_2^2 \\ &= (1 \oplus P_1^3 \oplus P_1^4 \oplus P_2^3 \oplus P_1^3 P_2^3 \oplus P_1^4 P_2^3) \oplus (P_2^3 \oplus P_1^4 P_2^3) \\ &= 1 \oplus P_1^3 \oplus P_1^4 \oplus \textcolor{red}{P_2^3} \oplus P_1^3 P_2^3 \oplus \textcolor{blue}{P_1^4 P_2^3} \oplus \textcolor{red}{P_2^3} \oplus \textcolor{blue}{P_1^4 P_2^3} \\ &= 1 \oplus P_1^3 \oplus P_1^4 \oplus P_1^3 P_2^3. \end{aligned}$$

The function F_2 can then be realized as a circuit, as shown in Fig. 15.

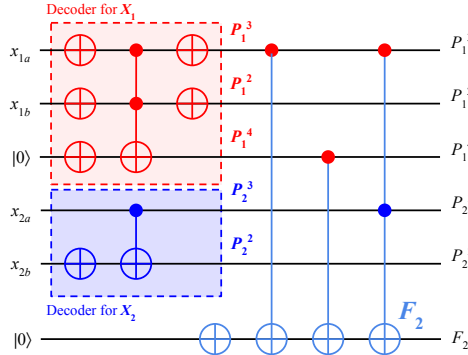


Figure 15: Circuit for F_2 realized with decoders from the MVI-FPRM form with polarity P_1, P_2 for Example 6.

The circuit in Fig. 15 has 7 NOT gates, 3 CNOT gates, and 2 3-bit Toffoli Gates. So, the Maslov cost is 20, and the TQC is 157.

The function F_2 , from Example 6, was expressed as $X_1^{0,2,3}X_2^{0,1} \oplus X_1^0X_2^2$. However, functions can be expressed in multiple ways, but the MVI-FPRM is unique for a function. This is shown in Example 7.

Example 7. Take the function F_2 from Example 6 with polarities P_1 and P_2 .

The Marquand chart of F_2 was drawn in Fig 14. The chart from this figure showed the groupings for the terms $X_1^{0,2,3}X_2^{0,1}$ and $X_1^0X_2^2$, which were the terms used to represent F_2 in Example 6.

However, there are more possible groupings. One such grouping is shown in Fig. 16.

The red group corresponds to the term $X_1^0 X_2^{0,1,2} = X_1^0$, and the blue group corresponds to the term $X_1^{2,3} X_2^{0,1}$. So

$$F_2 = X_1^0 \oplus X_1^{2,3} X_2^{0,1}.$$

The MVI-FPRM form of the first term, X_1^0 , is

$$\begin{aligned} X_1^0 &= X_1^{0,1,2,3} \oplus X_1^{1,2,3} \\ &= P_1^1 \oplus P_1^4 \\ &= 1 \oplus P_1^4. \end{aligned}$$

	X_2	0	1	2
0		1	1	1
1		0	0	0
2		1	1	0
3		1	1	0

$X_1^0 X_2^{0,1,2} \oplus X_1^{2,3} X_2^{0,1}$

Figure 16: Marquand chart of F_2 with a different grouping from Example 7.

And the MVI-FPRM form of the second term, $X_1^{2,3} X_2^{0,1}$ is

$$\begin{aligned} X_1^{2,3} X_2^{0,1} &= X_1^{2,3} (X_2^{0,1,2} \oplus X_2^2) \\ &= P_1^3 (P_2^1 \oplus P_2^3) \\ &= P_1^3 (1 \oplus P_2^3) \\ &= P_1^3 \oplus P_1^3 P_2^3. \end{aligned}$$

Combining the MVI-FPRM forms of the two terms gives the same form for F_2 that was found in Example 6: $1 \oplus P_1^3 \oplus P_1^4 \oplus P_1^3 P_2^3$.

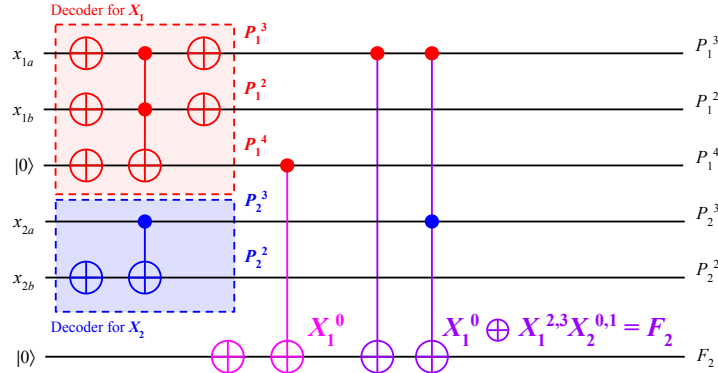


Figure 17: Circuit for F_2 realized from the terms X_1^0 and $X_1^{2,3} X_2^{0,1}$ from Example 7.

Constructing the circuit for F_2 , shown in Fig. 17, consists of 7 NOT gates, 3 CNOT gates, and 2 3-bit Toffoli gates and has a cost of 20 (Maslov) and 157 (TQC), which is the same as the circuit from Fig. 15. This example shows how the MVI-FPRM is a canonical form.

An important factor for the cost of the circuit is the polarity, which is demonstrated in Example 8.

Example 8. Take the function $F_2 = X_1^{0,2,3} X_2^{0,1} \oplus X_1^0 X_2^2 = X_1^0 \oplus X_1^{2,3} X_2^{0,1}$ from Example 6. Let's find the MVI-FPRM form of F_2 with the polarities:

$$Q_1 = \begin{bmatrix} 1 & 1 & 1 & 1 \\ 1 & 0 & 0 & 0 \\ 0 & 1 & 1 & 0 \\ 0 & 0 & 1 & 1 \end{bmatrix}, \quad Q_2 = \begin{bmatrix} 1 & 1 & 1 \\ 1 & 1 & 0 \\ 1 & 0 & 1 \end{bmatrix}.$$

The polarity literals for X_1 are

$$Q_1^1 = X_1^{0,1,2,3} = 1, \quad Q_1^2 = X_1^0, \quad Q_1^3 = X_1^{1,2}, \quad Q_1^4 = X_1^{2,3}.$$

And the polarity literals for X_2 are

$$Q_2^1 = X_2^{0,1,2} = 1, \quad Q_2^2 = X_2^{0,1}, \quad Q_2^3 = X_2^{0,2}.$$

It can be found that the MVI-FPRM form of F_2 is

$$\begin{aligned} F_2 &= X_1^0 \oplus X_1^{2,3} X_2^{0,1} \\ &= Q_1^2 \oplus Q_1^4 Q_2^2. \end{aligned}$$

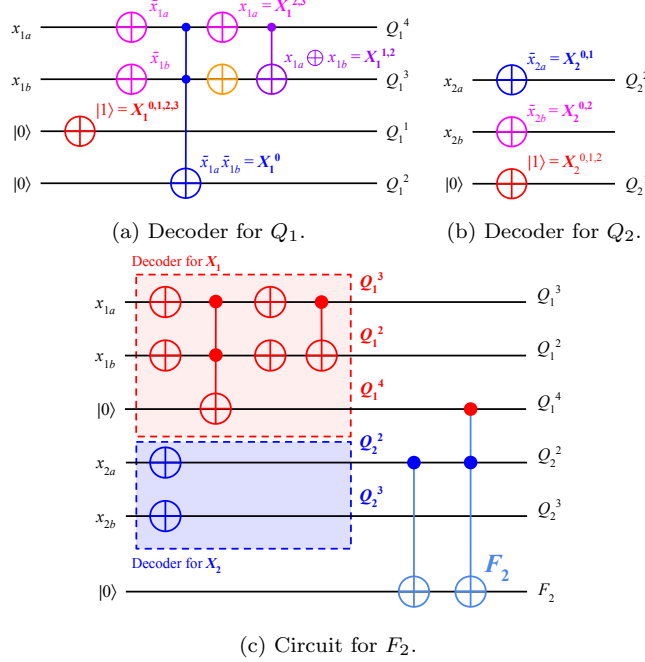


Figure 18: Decoders for Q_1 and Q_2 , and circuit for F_2 , for Example 8.

The decoder for X_1 with polarity Q_1 is realized in Fig. 18a, the decoder for X_2 with polarity Q_2 is realized in Fig. 18b, and the full circuit realization of F_2 is shown in Fig. 18c.

The resulting circuit has 6 NOT gates, 2 CNOT gates, and 2 3-bit Toffoli gates with a cost of 18 (Maslov) or 142 (TQC).

This shows that for the function F_2 , the polarities Q_1 and Q_2 lead to a less costly circuit than the polarities P_1 and P_2 . Thus, it is important to take into account what polarities to use depending on the function.

All the previous examples are single-output; however, this method is not restricted to single-output functions. This is presented in Example 9.

Example 9. Let F be a multi-output function which outputs F_1 (from Examples 4 and 5) and F_2 (from Example 6) with polarities Q_1 and Q_2 .

The MVI-FPRM form of the function F_1 is

$$\begin{aligned} F_1 &= X_1^{0,2,3} X_2^{0,1} \\ &= (X_1^0 \oplus X_1^{2,3})(X_2^{0,1}) \\ &= (Q_1^2 \oplus Q_1^4)(Q_2^2) \\ &= Q_1^2 Q_2^2 \oplus Q_1^4 Q_2^2. \end{aligned}$$

The MVI-FPRM form of F_2 was found in Example 8 to be

$$F_2 = Q_1^2 \oplus Q_1^4 Q_2^2.$$

The spectral coefficients of the two functions are listed in Table 10.

Coefficient	$M_{Q_1^4 Q_2^2}$										
Value for F_1	0	0	0	0	1	0	0	0	0	1	0
Value for F_2	0	0	0	1	0	0	0	0	0	1	0

Table 10: Spectrum of the functions F_1 and F_2 with polarities Q_1 and Q_2 for Example 9.

The multi-output function F can be realized as a circuit by first computing the shared terms, in this case the term $Q_1^4 Q_2^2$, and then computing the remaining individual output functions, as illustrated in Fig. 19. Note that the term $Q_1^4 Q_2^2$ is shared between F_1 and F_2 .

These methods can be applied to more complicated functions, such as the one in Example 10.

Example 10. Let $F_3 = X_4^1 X_5^{0,2} \oplus X_3^{1,2} X_4^{0,1} X_5^0 \oplus X_4^{0,2} X_5^{1,2} \oplus X_3^2 X_4^1 X_5^1$, where X_3 , X_4 , and X_5 are ternary variables.

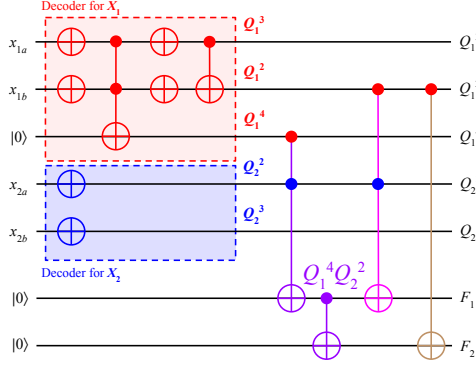


Figure 19: Circuit for F with outputs F_1 and F_2 from Example 9.

Let the polarities be

$$P_3 = \begin{bmatrix} 1 & 1 & 1 \\ 1 & 0 & 1 \\ 0 & 1 & 1 \end{bmatrix}, \quad P_4 = \begin{bmatrix} 1 & 1 & 1 \\ 1 & 1 & 0 \\ 0 & 1 & 0 \end{bmatrix}, \quad P_5 = \begin{bmatrix} 1 & 1 & 1 \\ 1 & 1 & 0 \\ 0 & 1 & 1 \end{bmatrix}.$$

Thus, the polarity literals for X_3 are

$$P_3^1 = X_3^{0,1,2} = 1, \quad P_3^2 = X_3^{0,2}, \quad P_3^3 = X_3^{1,2}.$$

The polarity literals for X_4 are

$$P_4^1 = X_4^{0,1,2} = 1, \quad P_4^2 = X_4^{0,1}, \quad P_4^3 = X_4^1.$$

The polarity literals for X_5 are

$$P_5^1 = X_5^{0,1,2} = 1, \quad P_5^2 = X_5^{0,1}, \quad P_5^3 = X_5^{1,2}.$$

The MVI-FPRM form of the function F_3 can be found to be

$$\begin{aligned} F_3 &= P_3^3 P_4^2 \oplus P_3^2 P_5^3 \oplus P_4^3 P_5^2 \\ &= X_3^{1,2} X_4^{0,1} \oplus X_3^{0,2} X_5^{1,2} \oplus X_4^1 X_5^{0,1} \end{aligned}$$

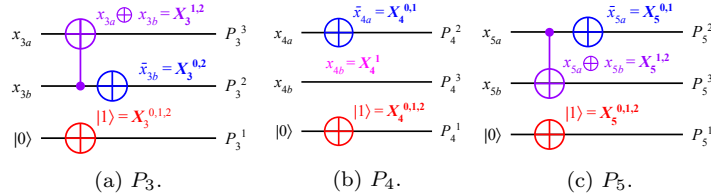


Figure 20: Decoders for P_3 , P_4 , and P_5 from Example 10.

The decoders for P_3 , P_4 , and P_5 are realized in Figs. 20a, 20b, and 20c. The full circuit for F_3 is illustrated in Fig. 21a. The function F_3 is shown on the Marquand charts in Fig. 21b and Fig. 21c. The rows and columns of a Marquand chart for over two variables are created by listing the possible values of X_3, X_4, X_5 in natural order.

The resulting circuit, which contains 2 NOT gates, 2 CNOT gates, and 3 3-bit Toffoli gates, has a Maslov cost of 19 and TQC of 192.

If, instead, the circuit was realized directly from the binary ESOP expression, then the result would be the circuit in Fig. 22, which contains 3 NOT gates, 2 CNOT gates, 1 3-bit Toffoli gate, and 5 4-bit Toffoli gates. This leads to a Maslov cost of 75 and TQC 630, which is more expensive than the MVI-FPRM-based circuit.

$$\begin{aligned} F_3 &= X_4^1 X_5^{0,2} \oplus X_3^{1,2} X_4^{0,1} X_5^0 \oplus X_4^{0,2} X_5^{1,2} \oplus X_3^2 X_4^1 X_5^1 \\ &= (x_{4b})(\bar{x}_{5b}) \oplus (x_{3a} \oplus x_{3b})(\bar{x}_{4a})(\bar{x}_{5a} \oplus x_{5b}) \oplus (\bar{x}_{4b})(x_{5a} \oplus x_{5b}) \oplus (x_{3a})(x_{4b})(x_{5b}) \\ &= x_{4b}\bar{x}_{5b} \oplus x_{3a}\bar{x}_{4a}\bar{x}_{5a} \oplus x_{3a}\bar{x}_{4a}x_{5b} \oplus x_{3b}\bar{x}_{4a}\bar{x}_{5a} \oplus x_{3b}\bar{x}_{4a}x_{5b} \oplus \bar{x}_{4b}x_{5a} \oplus \bar{x}_{4b}x_{5b} \oplus x_{3a}x_{4b}x_{5b} \\ &= x_{4b} \oplus x_{5b} \oplus x_{3a}\bar{x}_{4a}\bar{x}_{5a} \oplus x_{3a}\bar{x}_{4a}x_{5b} \oplus x_{3b}\bar{x}_{4a}\bar{x}_{5a} \oplus x_{3b}\bar{x}_{4a}x_{5b} \oplus \bar{x}_{4b}x_{5a} \oplus x_{3a}x_{4b}x_{5b} \end{aligned}$$

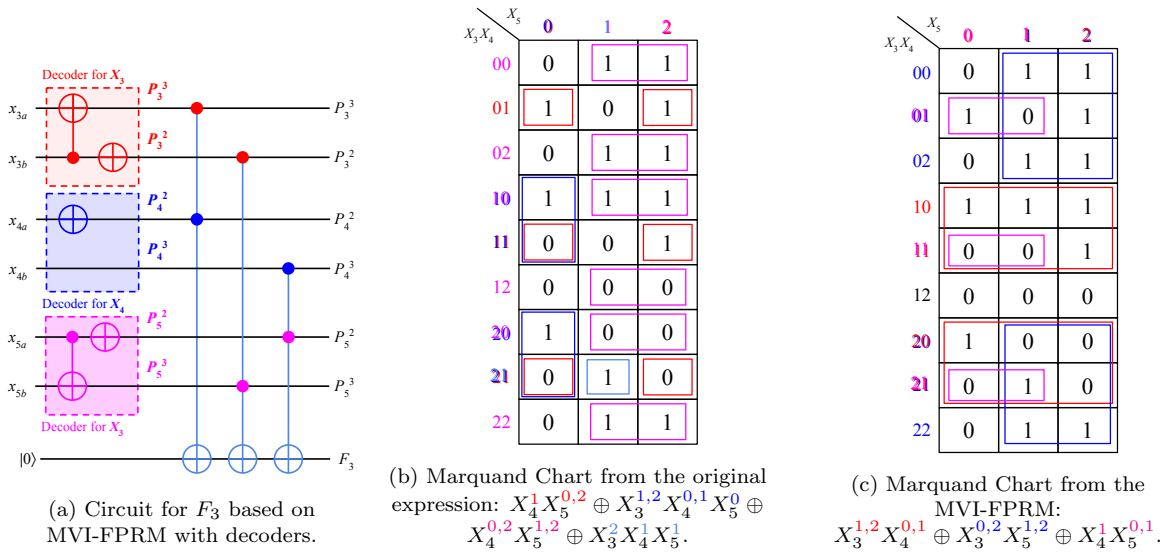


Figure 21: Circuit and Marquand chart for F_3 from Example 10.

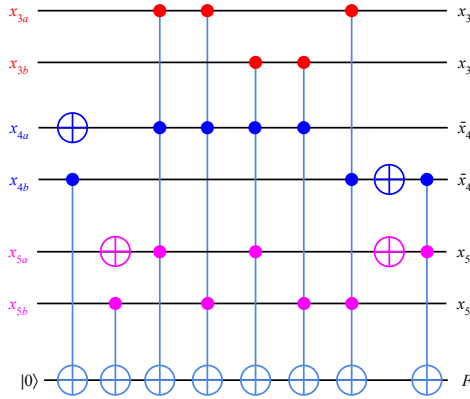


Figure 22: ESOP-based circuit for F_3 from Example 10.

The full process starting from binary variables is demonstrated in Example 11.

Example 11. Let $F_4 = x_a x_b \oplus \bar{x}_a x_b x_d \oplus x_c x_d \bar{x}_e \oplus \bar{x}_c \bar{x}_d \bar{x}_f$, where x_a, x_b, x_c, x_d, x_e , and x_f are binary variables.

The first step is to pair the binary variables to create multi-valued variables. Let the quaternary variable X_6 be encoded by x_a and x_b , let the quaternary variable X_7 be encoded by x_c and x_d , and let the quaternary variable X_8 be encoded by x_e and x_f .

Let the polarity be P_6, P_7, P_8 .

$$P_6 = \begin{bmatrix} 1 & 1 & 1 & 1 \\ 0 & 0 & 1 & 0 \\ 0 & 0 & 0 & 1 \\ 0 & 1 & 0 & 1 \end{bmatrix}, \quad P_7 = \begin{bmatrix} 1 & 1 & 1 & 1 \\ 1 & 0 & 0 & 0 \\ 0 & 0 & 0 & 1 \\ 0 & 1 & 0 & 1 \end{bmatrix}, \quad P_8 = \begin{bmatrix} 1 & 1 & 1 & 1 \\ 1 & 1 & 0 & 0 \\ 1 & 0 & 1 & 0 \\ 0 & 1 & 1 & 1 \end{bmatrix}.$$

The next step is to rewrite F_4 in terms of the polarity literals (with $P_6^1 = P_7^1 = P_8^1 = 1$).

$$\begin{aligned} F_4 &= x_a x_b \oplus \bar{x}_a x_b x_d \oplus x_c x_d \bar{x}_e \oplus \bar{x}_c \bar{x}_d \bar{x}_f \\ &= X_6^3 \oplus X_6^2 X_7^{1,3} \oplus X_7^3 X_8^{0,1} \oplus X_7^0 X_8^{0,2} \\ &= P_6^3 \oplus P_6^2 P_7^4 \oplus P_7^3 P_8^2 \oplus P_7^2 P_8^3 \end{aligned}$$

The function F_4 is realized with the circuit in Fig. 23a. This circuit consists of 3 NOT gates, 4 CNOT gates, and 6 3-bit Toffoli gates, and thus the circuit has a Maslov cost of 37 and a TQC of 383.

If the function F_4 was realized using the ESOP instead, then the resulting circuit, shown in Fig. 23b, would instead consist of 5 NOT gates, 1 3-bit Toffoli gate, and 3 4-bit Toffoli gates, and thus the circuit has a Maslov cost of 49 and a TQC of 386, making it more expensive than the MVI-FPRM-based circuit.

In summary, MVI functions can be transformed into a form analogous to the FPRM form from classical Reed-Muller logic, where each variable has a fixed polarity. In the case of MVI variables, the polarities are not just positive and negative, and instead there are many more options, as explained in Section 3.3.

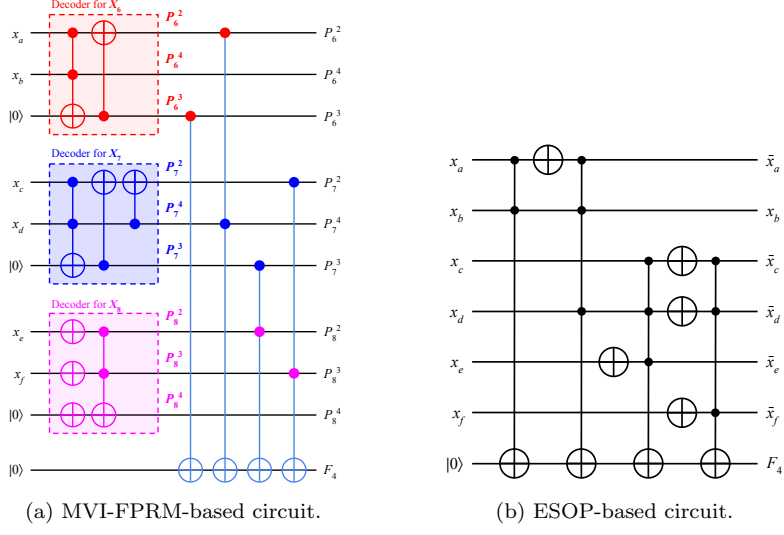


Figure 23: Circuits for F_4 from Example 11.

Polarities can be realized beforehand in a circuit by using decoders, as presented in Section 3.2, which are placed at the start of a circuit, and the outputs, the polarity literals, can be used to realize all possible functions. The cost of the decoders becomes negligible as the size of the circuit increases.

The main factors, which have been demonstrated by the examples in this section, that determine the cost of realizing an FPRM, are:

- **Polarity:** This affects the cost of the decoders and how many gates are needed to realize the terms. It is important to choose a suitable polarity for a function.
- **Pairings:** The specific binary variables that are paired to encode the multi-valued variables. There also may be more than two binary variables that encode a multi-valued variable (e.g., three binary variables can encode an 8-valued variable).

Comparisons between MVI-FPRM-based and ESOP-based circuits for F_3 and F_4 are summarized in Table 11.

Function	MVI-FPRM-Based						ESOP-Based					
	NOT	CNOT	3-bit Toffoli	4-bit Toffoli	Maslov Cost	TQC	NOT	CNOT	3-bit Toffoli	4-bit Toffoli	Maslov Cost	TQC
F_3	2	2	3	0	19	192	3	2	1	5	75	630
F_4	3	4	6	0	37	383	5	0	1	3	49	386

Table 11: MVI-FPRM-based vs ESOP-based circuits for F_3 and F_4 .

It is important to remember that MVI functions use multi-valued variables as a representation of multiple binary variables, and all the circuits and operations are binary, not multi-valued.

5 Products-Matching Method

We introduce a products-matching method to find the exact minimum MVI-FPRM form and the corresponding quantum circuit.

The method for finding the MVI-FPRM form includes two stages. In the first stage, every multi-valued literal is transformed to a polarity that is specified by the chosen linearly independent polarity matrix. In the second stage, the terms consisting of transformed literals are used to calculate the final MVI-FPRM form. The code for the transformation of a multiple-valued literal is selected in such a way that the second stage of the transformation does not depend on the polarity chosen for the literal. This approach requires the introduction of normalized codes.

5.1 Transformation of a Multi-Valued Input Literal

The basic steps of the method for the transformation of a multiple-valued literal to its representation of polarity literals in the normalized code will be illustrated in Example 12.

Example 12. The goal is to find the normalized code of the literal X^0 (where X is quaternary) with the polarity P .

$$P = \begin{bmatrix} 1 & 1 & 1 & 1 \\ 0 & 1 & 0 & 1 \\ 0 & 0 & 1 & 1 \\ 0 & 1 & 1 & 1 \end{bmatrix}$$

MVI Literal	Binary Code	Polarity Literal	Normalized Code
X^0	1000	P^1	1000
X^1	0100	P^2	0100
X^2	0010	P^3	0010
X^3	0001	P^4	0001

Table 12: Binary and normalized codes for Example 12. The binary code is based on the set of truth values of the MVI literal, while the normalized coder is based on the polarity literals.

The binary and normalized codes are listed in Table 12. The literal X^0 can be represented by the binary code 1000. X^0 can also be expressed as $P^1 \oplus P^4$, which has the normalized code 1001. The new code representing this combination of polarity literals can be derived by the bit-by-bit XOR operation of the code representation of the polarity literals. The normalized code has a ‘1’ in its bit representation corresponding to the index of the polarity literal P^r .

MVI Literal	XOR of Polarity Literals	Normalized Code
X^0	$P^1 \oplus P^4$	1001
X^1	$P^3 \oplus P^4$	0011
X^2	$P^2 \oplus P^4$	0101
X^3	$P^2 \oplus P^3 \oplus P^4$	0111

Table 13: MVI literals and their respective XOR expression with polarity literals and normalized codes, for Example 12.

The MVI literals X^0 , X^1 , X^2 , and X^3 are expressed in terms of the polarity literals and represented by a normalized code in Table 13. To find the normalized code of any MVI literal X^S , apply a bit-by-bit XOR operation on the normalized codes of all the literals X^r such that $r \in S$. For instance, the normalized code for $X^{0,1}$ is 1010, found by the bit-by-bit XOR of the codes 1001 (for X^0) and 0011 (for X^1).

The algorithm for transforming an MVI literal into its normalized code is described as follows, and is demonstrated in Table 14:

1. Generate all possible XOR combinations of the polarity literals P^r for later comparison with the original MVI literal (first row).
2. Compare the binary representation of the MVI literal with the binary representation of the XOR combination (second row and second column). If these two binary representations are equal, assign to the multiple-valued literal its normalized code (shown by marking a ‘1’ in the cell).

5.2 Transformation of a Multi-Valued Input Function

After the transformation of every original multiple-valued literal, as described in Section 5.1, the entire set of multiple-valued terms of the function has to be changed to the MVI-FPRM form. In our method, every product term of the input function is compared to the normalized code of the indices of all spectral coefficients.

The basic steps of the algorithm for the products-matching method are explained in Example 13.

Example 13. Let G be a function of the ternary variable X_1 , quaternary variable X_2 , and ternary variable X_3 . For the MVI-FPRM form of G , the variables have the polarities P_1 , P_2 , and P_3 , respectively.

The normalized codes corresponding to each spectral coefficient are stated in Table 15. It can be observed that the code for each spectral coefficient consists of a combination of the codes for three polarity literals, in which every polarity literal is taken from a different original multi-valued variable.

The final value of the spectral coefficient $M_{P_1^{r_1} P_2^{r_2} P_3^{r_3}}$, determined by a column from Table 15, is obtained by comparing the normalized codes of all product terms of the Boolean function with the

Literals	P^1	P^2	P^3	P^4	$P^1 \oplus P^2$
Binary Code	1111	0101	0011	0111	1010
$X^{0,2}$	1010				1
$X^{1,3}$	0101		1		
$X^{2,3}$	0011			1	
$X^{1,2,3}$	0111				1
$X^{0,1,2,3}$	1111	1			
Literals	$P^1 \oplus P^3$	$P^1 \oplus P^4$	$P^2 \oplus P^3$	$P^2 \oplus P^4$	$P^3 \oplus P^4$
Binary Code	1100	1000	0110	0010	0100
X^0	1000		1		
$X^{0,1}$	1100	1			
$X^{1,2}$	0110			1	
X^2	0010				1
X^1	0100				1
Literals	$P^1 \oplus P^2 \oplus P^3$	$P^1 \oplus P^2 \oplus P^4$	$P^1 \oplus P^3 \oplus P^4$	$P^2 \oplus P^3 \oplus P^4$	$P^1 \oplus P^2 \oplus P^3 \oplus P^4$
Binary Code	1001	1101	1011	0001	1110
X^3	0001			1	
$X^{0,3}$	1001	1			
$X^{0,1,2}$	1110				1
$X^{0,1,3}$	1101		1		
$X^{0,2,3}$	1011			1	

Table 14: Table for finding the MVI literals in terms of polarity literals using normalized codes, from Example 12.

M	$M_{P_1^1 P_2^1 P_3^1}$	$M_{P_1^1 P_2^1 P_3^2}$	$M_{P_1^1 P_2^1 P_3^3}$	$M_{P_1^1 P_2^2 P_3^1}$	$M_{P_1^1 P_2^2 P_3^2}$	\dots	$M_{P_1^3 P_2^4 P_3^3}$
Code	100 1000 100	100 1000 010	100 1000 001	100 0100 100	100 0100 010	\dots	001 0001 001

Table 15: The normalized code for the complete MVI-FPRM spectrum of the function G from Example 13.

variables X_1, X_2, \dots, X_n represented with normalized codes. The value $M_{P_1^{r_1} P_2^{r_2} P_3^{r_3}}$ is the representation of the output function, if the intersection (bit-by-bit AND operation) of the codes is not empty (no part of the code for a variable is all 0's). To obtain the final value $M_{P_1^{r_1} P_2^{r_2} P_3^{r_3}}$ for all terms of the function, the XOR operation has to be performed for all values $M_{P_1^{r_1} P_2^{r_2} P_3^{r_3}}$.

The final MVI-FPRM form includes terms that are obtained by replacing the polarity literals in the indices of the spectral coefficients, which have a value that is not 0, with their binary representation.

To summarize, the procedure for obtaining MVI-FPRM of a multi-output Boolean function can be described by the following algorithm:

1. Transform all the MVI literals of the function to their normalized codes according to the chosen polarities for the variables (algorithm in Section 5.1).
2. Calculate the MVI-FPRM spectrum for the normalized codes.
3. Replace the polarity literals of non-zero spectral coefficients by their original MVI literal. The output functions for the terms are given by the values of the spectral coefficients.

As one can observe, each spectral coefficient can be calculated in turn, which allows one to solve larger problems. In addition, every expression created by the program can be factorized and transformed to a form of MVI-GRM, which reduces the cost of the resulting quantum circuit.

6 MVI-FPRM-Based 2-Bit Adder

MVI-FPRM forms can be used practically to create quantum adders. Assume the binary variables x_a, x_b, x_c, x_d . The variables x_a and x_b are paired to create the quaternary variable X_1 , and x_c and x_d are paired to create X_2 , as stated in Table 16. The functions f_c , f_0 , and f_1 are represented by the Marquand charts in Fig. 24a, Fig. 24b, and Fig. 24c, respectively.

There are many possible polarities for realizing the adder, and this was only one possible pairing. This is a difficult search problem, since there are $6 \cdot 480^2$ possible pairings and polarities. This section will cover two possible solutions. The intention here is to present the cost differences between various solutions.

x_a, x_b	X_1	x_c, x_d	X_2	$f_c f_0 f_1$	x_a, x_b	X_1	x_c, x_d	X_2	$f_c f_0 f_1$
00	0	00	0	000	10	2	00	0	010
00	0	01	1	001	10	2	01	1	011
00	0	10	2	010	10	2	10	2	100
00	0	11	3	011	10	2	11	3	101
01	1	00	0	001	11	3	00	0	011
01	1	01	1	010	11	3	01	1	100
01	1	10	2	011	11	3	10	2	101
01	1	11	3	100	11	3	11	3	110

Table 16: Truth table for a 2-bit MVI adder.

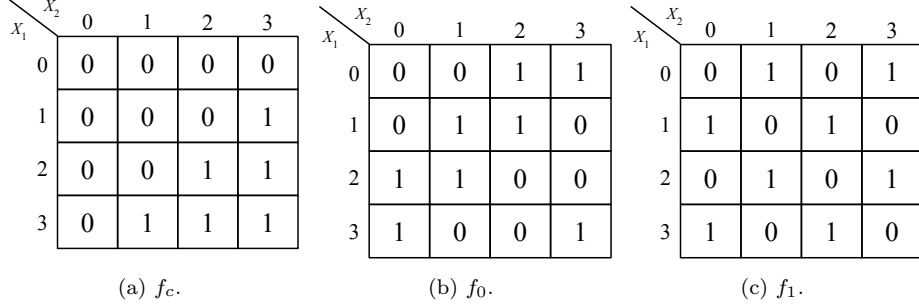


Figure 24: Marquand charts for f_c , f_0 , and f_1 .

6.1 First Possible 2-Bit Adder

Let X_1 and X_2 have the polarities P_1 and P_2 respectively.

$$P_1 = \begin{bmatrix} 1 & 1 & 1 & 1 \\ 0 & 1 & 0 & 1 \\ 0 & 0 & 1 & 0 \\ 1 & 1 & 0 & 0 \end{bmatrix}, \quad P_2 = \begin{bmatrix} 1 & 1 & 1 & 1 \\ 0 & 1 & 0 & 1 \\ 0 & 0 & 1 & 0 \\ 1 & 1 & 0 & 0 \end{bmatrix}$$

X_1	X_2	Binary Code	Normalized Code	$f_c f_0 f_1$	X_1	X_2	Binary Code	Normalized Code	$f_c f_0 f_1$
0	0	1000 1000	1110 1110	000	2	0	0010 1000	0010 1110	010
0	1	1000 0100	1110 1111	001	2	1	0010 0100	0010 1111	011
0	2	1000 0010	1110 0010	010	2	2	0010 0010	0010 0010	100
0	3	1000 0001	1110 1011	011	2	3	0010 0001	0010 1011	101
1	0	0100 1000	1111 1110	001	3	0	0001 1000	1011 1110	011
1	1	0100 0100	1111 1111	010	3	1	0001 0100	1011 1111	100
1	2	0100 0010	1111 0010	011	3	2	0001 0010	1011 0010	101
1	3	0100 0001	1111 1011	100	3	3	0001 0001	1011 1011	110

Table 17: Normalized codes for a 2-bit MVI adder with the polarities P_1 and P_2 .

The products-matching method can be applied to obtain an MVI-FPRM form, which then can be realized as a binary quantum circuit.

Step 1: Transform all the MVI literals of the function to their normalized codes according to the chosen polarities for the variables.

The literals are $X_i^0 = P_i^1 \oplus P_i^2 \oplus P_i^3$ (normalized code 1110), $X_i^1 = P_i^1 \oplus P_i^2 \oplus P_i^3 \oplus P_i^4$ (normalized code 1111), $X_i^2 = P_i^3$ (normalized code 0010), and $X_i^3 = P_i^1 \oplus P_i^3 \oplus P_i^4$ (normalized code 1011). The codes for all the potential inputs are listed in Table 17.

Step 2: Calculate the MVI-FPRM spectrum for the normalized codes.

The normalized code obtained in the previous step is now compared with all the indices of the spectral coefficients of the general spectrum for the adder functions.

The calculation of the MVI spectrum for Table 17 is illustrated in Table 18. The table has the output functions of the terms as entries (in the order $f_c f_0 f_1$) with the intersection of the term in each cell.

For instance, the cell for the intersection of row 1110 1011 and column 0100 1000 is ‘011’. This is because the bit-by-bit intersection (AND operation) of the indices is 0100 1000, so both literals are not empty, thus the value of the cell is equal to the outputs of f_c , f_0 , and f_1 for the normalized code 1110 1011, which is stated in the fourth row of Table 17 to be 011.

Term	$M_{P_1^1 P_2^1}$ 1000 1000	$M_{P_1^1 P_2^2}$ 1000 0100	$M_{P_1^1 P_2^3}$ 1000 0010	$M_{P_1^1 P_2^4}$ 1000 0001	$M_{P_1^2 P_2^1}$ 0100 1000	$M_{P_1^2 P_2^2}$ 0100 0100	$M_{P_1^2 P_2^3}$ 0100 0010	$M_{P_1^2 P_2^4}$ 0100 0001
1110 1110	000	000	000	—	000	000	000	—
1110 1111	001	001	001	001	001	001	001	001
1110 0010	—	—	010	—	—	—	010	—
1110 1011	011	—	011	011	011	—	011	011
1111 1110	001	001	001	—	001	001	001	—
1111 1111	010	010	010	010	010	010	010	010
1111 0010	—	—	011	—	—	—	011	—
1111 1011	100	—	100	100	100	—	100	100
0010 1110	—	—	—	—	—	—	—	—
0010 1111	—	—	—	—	—	—	—	—
0010 0010	—	—	—	—	—	—	—	—
0010 1011	—	—	—	—	—	—	—	—
1011 1110	011	011	011	—	—	—	—	—
1011 1111	100	100	100	100	—	—	—	—
1011 0010	—	—	101	—	—	—	—	—
1011 1011	110	—	110	110	—	—	—	—
Result	100	101	000	110	101	010	100	100
Term	$M_{P_1^3 P_2^1}$ 0010 1000	$M_{P_1^3 P_2^2}$ 0010 0100	$M_{P_1^3 P_2^3}$ 0010 0010	$M_{P_1^3 P_2^4}$ 0010 0001	$M_{P_1^4 P_2^1}$ 0001 1000	$M_{P_1^4 P_2^2}$ 0001 0100	$M_{P_1^4 P_2^3}$ 0001 0010	$M_{P_1^4 P_2^4}$ 0001 0001
1110 1110	000	000	000	—	—	—	—	—
1110 1111	001	001	001	001	—	—	—	—
1110 0010	—	—	010	—	—	—	—	—
1110 1011	011	—	011	011	—	—	—	—
1111 1110	001	001	001	—	001	001	001	—
1111 1111	010	010	010	010	010	010	010	010
1111 0010	—	—	011	—	—	—	011	—
1111 1011	100	—	100	100	100	—	100	100
0010 1110	010	010	010	—	—	—	—	—
0010 1111	011	011	011	011	—	—	—	—
0010 0010	—	—	100	—	—	—	—	—
0010 1011	101	—	101	101	—	—	—	—
1011 1110	011	011	011	—	011	011	011	—
1011 1111	100	100	100	100	100	100	100	100
1011 0010	—	—	101	—	—	—	101	—
1011 1011	110	—	110	110	110	—	110	110
Result	000	100	000	000	110	100	000	100

Table 18: Spectrum of the adder from Table 17.

The intersection of row 1110 0010 and column 0100 1000 is 0100 0000, so ‘—’ is placed in the corresponding cell because 0000 appears (the literal is empty). The final coefficients for the functions in Table 18 are obtained by the bit-by-bit XOR operation on the entries of the columns.

From Table 18, it can be found that the functions f_c , f_0 , and f_1 are

$$\begin{aligned} f_c &= P_1^1 P_2^1 \oplus P_1^1 P_2^2 \oplus P_1^1 P_2^4 \oplus P_1^2 P_2^1 \oplus P_1^2 P_2^3 \oplus P_1^2 P_2^4 \oplus P_1^3 P_2^2 \oplus P_1^4 P_2^1 \oplus P_1^4 P_2^2 \oplus P_1^4 P_2^4 \\ f_0 &= P_1^1 P_2^4 \oplus P_1^2 P_2^2 P_1^4 P_2^1 \\ f_1 &= P_1^1 P_2^2 \oplus P_1^2 P_2^1. \end{aligned}$$

Step 3: Replace the polarity literals of non-zero spectral coefficients by their original MVI literal. The output functions for the terms are given by the values of the spectral coefficients. Replacing the polarity literals with the original MVI literals yields the MVI-FPRM forms of the functions.

$$\begin{aligned} f_c &= 1 \oplus X_2^{1,3} \oplus X_2^{0,1} \oplus X_1^{1,3} \oplus X_1^{1,3} X_2^2 \oplus X_1^{1,3} X_2^{0,1} \oplus X_1^2 X_2^{1,3} \oplus X_1^{0,1} \oplus X_1^{0,1} X_2^{1,3} \oplus X_1^{0,1} X_2^{0,1} \\ f_0 &= X_2^{0,1} \oplus X_1^{1,3} X_2^{1,3} \oplus X_1^{0,1} \\ f_1 &= X_2^{1,3} \oplus X_1^{1,3}. \end{aligned}$$

From the products-matching method, the MVI-FPRM forms (replacing P_1^1 and P_2^1 with 1) for f_c , f_0 , and f_1 are

$$\begin{aligned} f_c &= 1 \oplus \textcolor{red}{P_2^2} \oplus \textcolor{blue}{P_2^4} \oplus \textcolor{red}{P_1^2} \oplus P_1^2 P_2^3 \oplus P_1^2 P_2^4 \oplus P_1^3 P_2^2 \oplus \textcolor{teal}{P_1^4} \oplus P_1^4 P_2^2 \oplus P_1^4 P_2^4 \\ f_0 &= \textcolor{blue}{P_2^4} \oplus P_1^2 P_2^2 \oplus \textcolor{teal}{P_1^4} \\ f_1 &= \textcolor{red}{P_2^2} \oplus \textcolor{red}{P_1^2}. \end{aligned}$$

The adder is realized as a quantum circuit in Fig. 25. It is made up of 7 NOT gates, 6 CNOT gates, and 8 3-bit Toffoli gates. The circuit has a Maslov cost of 53 and a TQC of 523. Note that all n -bit Toffoli gates are at most $n = 3$.

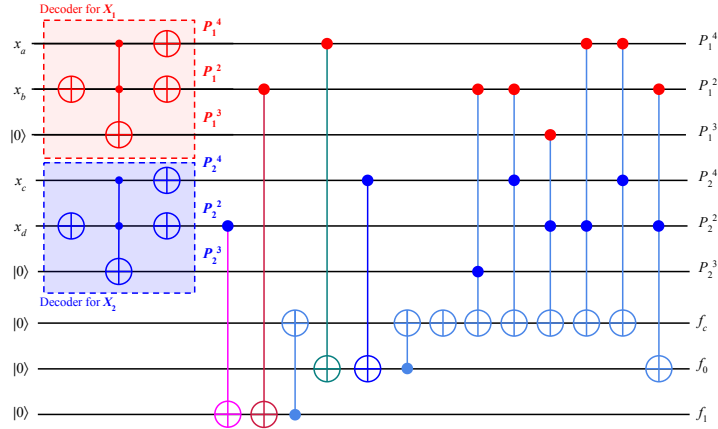


Figure 25: The 2-bit quantum adder based on the MVI-FPRM with the polarity P_1, P_2 .

6.2 Second Possible 2-Bit Adder

For the second possible solution, let X_1 and X_2 instead have the polarities Q_1 and Q_2 respectively.

$$Q_1 = \begin{bmatrix} 1 & 1 & 1 & 1 \\ 0 & 1 & 1 & 0 \\ 0 & 0 & 1 & 0 \\ 1 & 1 & 0 & 0 \end{bmatrix}, \quad Q_2 = \begin{bmatrix} 1 & 1 & 1 & 1 \\ 0 & 1 & 1 & 0 \\ 0 & 0 & 1 & 0 \\ 1 & 1 & 0 & 0 \end{bmatrix}$$

X_1	X_2	Binary Code	Normalized Code	$f_c f_0 f_1$	X_1	X_2	Binary Code	Normalized Code	$f_c f_0 f_1$
0	0	1000 1000	0111 0111	000	2	0	0010 1000	0010 0111	010
0	1	1000 0100	0111 0110	001	2	1	0010 0100	0010 0110	011
0	2	1000 0010	0111 0010	010	2	2	0010 0010	0010 0010	100
0	3	1000 0001	0111 1011	011	2	3	0010 0001	0010 1011	101
1	0	0100 1000	0110 0111	001	3	0	0001 1000	1011 0111	011
1	1	0100 0100	0110 0110	010	3	1	0001 0100	1011 0110	100
1	2	0100 0010	0110 0010	011	3	2	0001 0010	1011 0010	101
1	3	0100 0001	0110 1011	100	3	3	0001 0001	1011 1011	110

Table 19: Normalized codes for a 2-bit MVI adder with the polarities Q_1 and Q_2 .

Step 1: Transform all the MVI literals of the function to their normalized codes according to the chosen polarities for the variables.

The literals are $X_i^0 = Q_i^2 \oplus Q_i^3 \oplus Q_i^4$ (normalized code 0111), $X_i^1 = Q_i^1 \oplus Q_i^3$ (normalized code 0110), $X_i^2 = Q_i^3$ (normalized code 0010), and $X_i^3 = Q_i^1 \oplus Q_i^3 \oplus Q_i^4$ (normalized code 1011). The codes for all the potential inputs are listed in Table 19.

Step 2: Calculate the MVI-FPRM spectrum for the normalized codes.

The calculation of the MVI spectrum for Table 19 is illustrated in Table 20. From Table 20, it can be found that the functions f_c , f_0 , and f_1 are

$$\begin{aligned}
f_c &= Q_1^1 Q_2^1 \oplus Q_1^1 Q_2^2 \oplus Q_1^1 Q_2^3 \oplus Q_1^1 Q_2^4 \oplus Q_1^2 Q_2^1 \oplus Q_1^2 Q_2^3 \oplus Q_1^2 Q_2^4 \oplus Q_1^3 Q_2^1 \oplus Q_1^3 Q_2^2 \oplus Q_1^3 Q_2^4 \oplus Q_1^4 Q_2^1 \oplus Q_1^4 Q_2^2 \\
&\quad \oplus Q_1^4 Q_2^3 \oplus Q_1^4 Q_2^4 \\
f_0 &= Q_1^1 Q_2^1 \oplus Q_1^1 Q_2^2 \oplus Q_1^2 Q_2^1 \oplus Q_1^2 Q_2^2 \oplus Q_1^2 Q_2^4 \oplus Q_1^4 Q_2^2 \oplus Q_1^4 Q_2^4 \\
f_1 &= Q_1^1 Q_2^2 \oplus Q_1^1 Q_2^4 \oplus Q_1^2 Q_2^1 \oplus Q_1^4 Q_2^1.
\end{aligned}$$

Step 3: Replace the polarity literals of non-zero spectral coefficients by their original MVI literal. The output functions for the terms are given by the values of the spectral coefficients. Replacing the polarity literals with the original MVI literals yields the MVI-FPRM forms of the functions.

$$\begin{aligned}
f_c &= 1 \oplus X_2^{1,2} \oplus X_2^2 \oplus X_2^{0,1} \oplus X_1^{1,2} \oplus X_1^{1,2} X_2^2 \oplus X_1^{1,2} X_2^{0,1} \oplus X_1^2 \oplus X_1^2 X_2^{1,2} \oplus X_1^2 X_2^{0,1} \oplus X_1^{0,1} \oplus X_1^{0,1} X_2^{1,2} \\
&\quad \oplus X_1^{0,1} X_2^2 \oplus X_1^{0,1} X_2^{0,1} \\
f_0 &= 1 \oplus X_2^{1,2} \oplus X_1^{1,2} \oplus X_1^{1,2} X_2^{1,2} \oplus X_1^{1,2} X_2^{0,1} \oplus X_1^{0,1} X_2^{1,2} \oplus X_1^{0,1} X_2^{0,1} \\
f_1 &= X_2^{1,2} \oplus X_2^{0,1} \oplus X_1^{1,2} \oplus X_1^{0,1}.
\end{aligned}$$

Term	$M_{Q_1^1 Q_2^1}$ 1000 1000	$M_{Q_1^1 Q_2^2}$ 1000 0100	$M_{Q_1^1 Q_2^3}$ 1000 0010	$M_{Q_1^1 Q_2^4}$ 1000 0001	$M_{Q_1^2 Q_2^1}$ 0100 1000	$M_{Q_1^2 Q_2^2}$ 0100 0100	$M_{Q_1^2 Q_2^3}$ 0100 0010	$M_{Q_1^2 Q_2^4}$ 0100 0001
0111 0111	—	—	—	—	—	000	000	000
0111 0110	—	—	—	—	—	001	001	—
0111 0010	—	—	—	—	—	—	010	—
0111 1011	—	—	—	—	011	—	011	011
0110 0111	—	—	—	—	—	001	001	001
0110 0110	—	—	—	—	—	010	010	—
0110 0010	—	—	—	—	—	—	011	—
0110 1011	—	—	—	—	100	—	100	100
0010 0111	—	—	—	—	—	—	—	—
0010 0110	—	—	—	—	—	—	—	—
0010 0010	—	—	—	—	—	—	—	—
0010 1011	—	—	—	—	—	—	—	—
1011 0111	—	011	011	011	—	—	—	—
1011 0110	—	100	100	—	—	—	—	—
1011 0010	—	—	101	—	—	—	—	—
1011 1011	110	—	110	110	—	—	—	—
Result	110	111	100	101	111	010	100	110
Term	$M_{Q_1^3 Q_2^1}$ 0010 1000	$M_{Q_1^3 Q_2^2}$ 0010 0100	$M_{Q_1^3 Q_2^3}$ 0010 0010	$M_{Q_1^3 Q_2^4}$ 0010 0001	$M_{Q_1^4 Q_2^1}$ 0001 1000	$M_{Q_1^4 Q_2^2}$ 0001 0100	$M_{Q_1^4 Q_2^3}$ 0001 0010	$M_{Q_1^4 Q_2^4}$ 0001 0001
0111 0111	—	000	000	000	—	000	000	000
0111 0110	—	001	001	—	—	001	001	—
0111 0010	—	—	010	—	—	—	010	—
0111 1011	011	—	011	011	011	—	011	011
0110 0111	—	001	001	001	—	—	—	—
0110 0110	—	010	010	—	—	—	—	—
0110 0010	—	—	011	—	—	—	—	—
0110 1011	100	—	100	100	—	—	—	—
0010 0111	—	010	010	010	—	—	—	—
0010 0110	—	011	011	—	—	—	—	—
0010 0010	—	—	100	—	—	—	—	—
0010 1011	101	—	101	101	—	—	—	—
1011 0111	—	011	011	011	—	011	011	011
1011 0110	—	100	100	—	—	100	100	—
1011 0010	—	—	101	—	—	—	101	—
1011 1011	110	—	110	110	110	—	110	110
Result	100	100	100	100	101	110	100	110

Table 20: Spectrum of the adder from Table 19.

From the products-matching method, the MVI-FPRM forms (replacing P_1^1 and P_2^1 with 1) for f_c , f_0 , and f_1 are

$$\begin{aligned}
 f_c &= 1 \oplus Q_2^2 \oplus Q_2^3 \oplus Q_2^4 \oplus Q_1^2 \oplus Q_1^2 Q_2^3 \oplus Q_1^2 Q_2^4 \oplus Q_1^3 \oplus Q_1^3 Q_2^2 \oplus Q_1^3 Q_2^4 \oplus Q_1^4 \oplus Q_1^4 Q_2^2 \oplus Q_1^4 Q_2^3 \oplus Q_1^4 Q_2^4 \\
 f_0 &= 1 \oplus Q_2^2 \oplus Q_1^2 \oplus Q_1^2 Q_2^2 \oplus Q_1^2 Q_2^4 \oplus Q_1^4 Q_2^2 \oplus Q_1^4 Q_2^4 \\
 f_1 &= Q_2^2 \oplus Q_2^4 \oplus Q_1^2 \oplus Q_1^4.
 \end{aligned}$$

The adder is realized as a quantum circuit in Fig. 26, which consists of 5 NOT gates, 12 CNOT gates, and 10 3-bit Toffoli gates. The circuit has a Maslov cost of 67 and a TQC of 713.

7 Butterfly Diagram Method

This paper also introduces a design method based on butterfly diagrams [30,31,35,49] for MVI-FPRM forms that transform *minterms*, terms that contain single-valued literals of every variable, to a polarity. This is a method analogous to the binary FPRM butterfly in Section 2.6.

One example of a butterfly diagram is shown in Fig. 27a, which transforms the minterms of two ternary variables X_1 and X_2 to the polarity P_1, P_2 with literals $X_i^0, X_i^1, X_i^{0,1,2} = 1$. The values shown in the butterfly diagram transform $X_1^0 X_2^0 \oplus X_1^1 X_2^1 \oplus X_1^1 X_2^2$ to $X_1^0 X_2^0 \oplus X_1^1 X_2^0 \oplus X_1^1$. The values of this function are illustrated in the Marquand chart in Fig. 27b. In this case, both variables are of the same polarity, but diagrams can be created for variables with various polarities. For a function of n ternary variables, there 28^n possible butterfly diagrams, out of which the best solutions are selected. Note that another solution for this function is $X_1^0 \oplus X_1^{0,1} X_2^{1,2}$, which is an MVI-GRM.

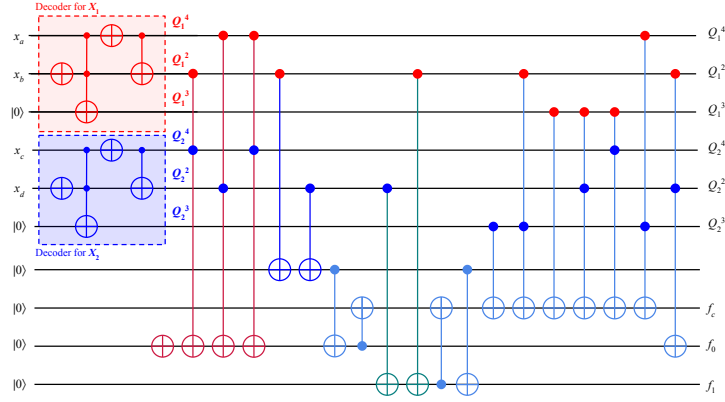


Figure 26: The 2-bit quantum adder based on the MVI-FPRM with the polarities Q_1 and Q_2 .

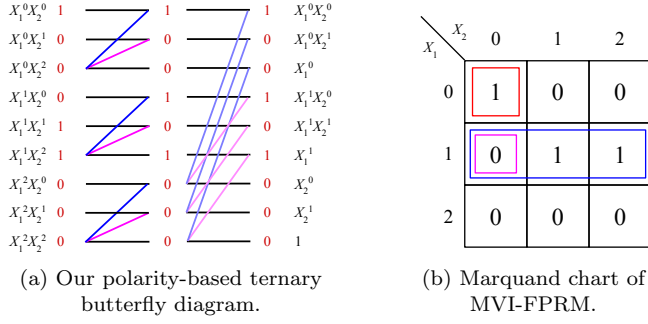


Figure 27: Example of butterfly diagram for $X_1^0X_2^0 \oplus X_1^1X_2^1 \oplus X_1^2X_2^2 = X_1^0X_2^0 \oplus X_1^1X_2^0 \oplus X_1^1$ with the corresponding Marquand chart.

Example 14. Let the variable X be ternary. The single-valued literals for X are X^0 , X^1 , and X^2 . The polarity matrix for this example is P . The goal is to create a butterfly diagram that transforms an XOR of the minterms (for one variable, the minterms are essentially just the single-valued literals) to the MVI-FPRM form for a function of a single ternary variable. This diagram can then be generalized to MVI functions with multiple variables.

$$P = \begin{bmatrix} 1 & 0 & 0 \\ 1 & 1 & 0 \\ 1 & 0 & 1 \end{bmatrix}$$

Any MVI function of one variable can be expressed in the form

$$f = a_0X^0 \oplus a_1X^1 \oplus a_2X^2.$$

Note that this form is equivalent to the ternary input Shannon expansion in Eq. (13) from Section 3.4, where the cofactors $f_{X=k} = a_k$. The coefficients a_0 , a_1 , and a_2 are the inputs to the butterfly diagram.

The single-valued literals are expressed in terms of the polarity literals as follows:

$$\begin{aligned} X^0 &= P^1 \\ X^1 &= P^1 \oplus P^2 \\ X^2 &= P^1 \oplus P^3. \end{aligned}$$

The single-valued literals can be substituted as polarity literals to yield a new expression for f .

$$\begin{aligned} f &= a_0X^0 \oplus a_1X^1 \oplus a_2X^2 \\ &= a_0(P^1) \oplus a_1(P^1 \oplus P^2) \oplus a_2(P^1 \oplus P^3) \\ &= a_0P^1 \oplus a_1P^1 \oplus a_1P^2 \oplus a_2P^1 \oplus a_2P^3 \\ &= a_0P^1 \oplus a_1P^1 \oplus a_2P^1 \oplus a_1P^2 \oplus a_2P^3 \\ &= (a_0 \oplus a_1 \oplus a_2)P^1 \oplus a_1P^2 \oplus a_2P^3 \\ &= M_{P1}P^1 \oplus M_{P2}P^2 \oplus M_{P3}P^3 \end{aligned}$$

This expansion, which is equivalent to the ternary input Davio-like expansion for the polarity P , which was found in Eq. (15), finds that spectral coefficients, which are the outputs of the butterfly diagram, are

$$\begin{aligned} M_{P1} &= a_0 \oplus a_1 \oplus a_2 \\ M_{P2} &= a_1 \\ M_{P3} &= a_2. \end{aligned}$$

The butterfly diagram for P is shown in Fig. 28.

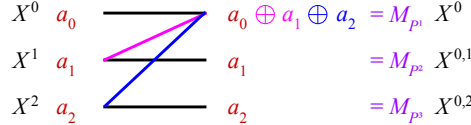


Figure 28: Butterfly diagram for P with a single ternary variable, X , for Example 14.

The same process from Example 14 can be applied for all polarities and radices. The butterfly diagram that transforms an XOR of minterms to the MVI-FPRM form for a single ternary variable for each polarity is listed in Table 21.

Polarity	Butterfly Diagram						
$\begin{bmatrix} 1 & 0 & 0 \\ 0 & 1 & 0 \\ 0 & 0 & 1 \end{bmatrix}$	—	$\begin{bmatrix} 1 & 0 & 0 \\ 1 & 1 & 0 \\ 0 & 0 & 1 \end{bmatrix}$	—	$\begin{bmatrix} 1 & 0 & 0 \\ 0 & 1 & 0 \\ 0 & 1 & 1 \end{bmatrix}$	—	$\begin{bmatrix} 1 & 0 & 0 \\ 1 & 1 & 0 \\ 1 & 1 & 1 \end{bmatrix}$	—
$\begin{bmatrix} 1 & 0 & 0 \\ 0 & 1 & 0 \\ 1 & 0 & 1 \end{bmatrix}$	—	$\begin{bmatrix} 1 & 0 & 0 \\ 1 & 1 & 0 \\ 1 & 0 & 1 \end{bmatrix}$	—	$\begin{bmatrix} 1 & 0 & 0 \\ 0 & 1 & 0 \\ 1 & 1 & 1 \end{bmatrix}$	—	$\begin{bmatrix} 1 & 0 & 0 \\ 1 & 1 & 0 \\ 0 & 1 & 1 \end{bmatrix}$	—
$\begin{bmatrix} 1 & 1 & 0 \\ 0 & 1 & 0 \\ 0 & 0 & 1 \end{bmatrix}$	—	$\begin{bmatrix} 1 & 0 & 0 \\ 0 & 1 & 1 \\ 0 & 0 & 1 \end{bmatrix}$	—	$\begin{bmatrix} 1 & 1 & 1 \\ 0 & 1 & 1 \\ 0 & 0 & 1 \end{bmatrix}$	—	$\begin{bmatrix} 1 & 0 & 0 \\ 1 & 1 & 1 \\ 0 & 0 & 1 \end{bmatrix}$	—
$\begin{bmatrix} 1 & 1 & 0 \\ 0 & 1 & 0 \\ 0 & 1 & 1 \end{bmatrix}$	—	$\begin{bmatrix} 0 & 1 & 1 \\ 1 & 1 & 1 \\ 1 & 1 & 0 \end{bmatrix}$	—	$\begin{bmatrix} 1 & 1 & 0 \\ 0 & 1 & 0 \\ 1 & 1 & 1 \end{bmatrix}$	—	$\begin{bmatrix} 1 & 0 & 0 \\ 1 & 1 & 1 \\ 1 & 0 & 1 \end{bmatrix}$	—
$\begin{bmatrix} 1 & 1 & 0 \\ 0 & 1 & 0 \\ 1 & 0 & 1 \end{bmatrix}$	—	$\begin{bmatrix} 1 & 0 & 0 \\ 0 & 1 & 1 \\ 1 & 0 & 1 \end{bmatrix}$	—	$\begin{bmatrix} 1 & 0 & 1 \\ 0 & 1 & 0 \\ 0 & 0 & 1 \end{bmatrix}$	—	$\begin{bmatrix} 1 & 0 & 1 \\ 1 & 1 & 1 \\ 0 & 0 & 1 \end{bmatrix}$	—
$\begin{bmatrix} 1 & 1 & 1 \\ 0 & 1 & 0 \\ 0 & 0 & 1 \end{bmatrix}$	—	$\begin{bmatrix} 1 & 1 & 1 \\ 0 & 1 & 0 \\ 0 & 0 & 1 \end{bmatrix}$	—	$\begin{bmatrix} 1 & 0 & 1 \\ 0 & 1 & 1 \\ 0 & 0 & 1 \end{bmatrix}$	—	$\begin{bmatrix} 1 & 1 & 0 \\ 0 & 1 & 1 \\ 0 & 0 & 1 \end{bmatrix}$	—
$\begin{bmatrix} 1 & 0 & 1 \\ 1 & 1 & 0 \\ 0 & 0 & 1 \end{bmatrix}$	—	$\begin{bmatrix} 1 & 0 & 1 \\ 0 & 1 & 0 \\ 0 & 1 & 1 \end{bmatrix}$	—	$\begin{bmatrix} 0 & 1 & 1 \\ 1 & 0 & 1 \\ 1 & 1 & 1 \end{bmatrix}$	—	$\begin{bmatrix} 1 & 1 & 0 \\ 1 & 0 & 1 \\ 1 & 1 & 1 \end{bmatrix}$	—

Table 21: All single-variable butterfly diagrams for the transformations to ternary input polarities.

To create the MVI-FPRM butterfly diagram for the ternary input function $F(X_1, X_2, \dots, X_n)$ with polarity P_1, P_2, \dots, P_n :

- The inputs represent the coefficients of the minterms, listed in natural order.
- The butterfly diagram is formed from n columns for each variable in descending order $(X_n, X_{n-1}, \dots, X_1)$.
 - The k th column transforms the single-valued literals of the variable X_{n-k+1} to the polarity P_{n-k+1} .
 - The k th column will be constructed with 3^k kernels, based on the polarity.
- The outputs represent the spectral coefficients of the polarity terms, listed in natural order.

This method can be extended to any radix. This is demonstrated in Example 15.

Example 15. Take the function $F_3 = X_4^1 X_5^{0,2} \oplus X_3^{1,2} X_4^{0,1} X_5^0 \oplus X_4^{0,2} X_5^{1,2} \oplus X_3^2 X_4^1 X_5^1$ from Example 10. Recall that the polarities used in Example 10 were P_3 , P_4 , and P_5 .

$$P_3 = \begin{bmatrix} 1 & 1 & 1 \\ 1 & 0 & 1 \\ 0 & 1 & 1 \end{bmatrix}, \quad P_4 = \begin{bmatrix} 1 & 1 & 1 \\ 1 & 1 & 0 \\ 0 & 1 & 0 \end{bmatrix}, \quad P_5 = \begin{bmatrix} 1 & 1 & 1 \\ 1 & 1 & 0 \\ 0 & 1 & 1 \end{bmatrix}$$

To fit the matrices to those of Table 21, the polarities will be redefined as Q_3 , Q_4 , Q_5 , where the rows are reordered.

$$Q_3 = \begin{bmatrix} 0 & 1 & 1 \\ 1 & 0 & 1 \\ 1 & 1 & 1 \end{bmatrix}, \quad Q_4 = \begin{bmatrix} 1 & 1 & 0 \\ 0 & 1 & 0 \\ 1 & 1 & 1 \end{bmatrix}, \quad Q_5 = \begin{bmatrix} 0 & 1 & 1 \\ 1 & 1 & 1 \\ 1 & 1 & 0 \end{bmatrix}$$

The function F_3 can be expanded to yield an equivalent expression with only minterms. The same expression can also be found through the Marquand Chart (Fig. 21c from Example 10).

$$\begin{aligned}
F_3 &= X_4^1 X_5^{0,2} \oplus X_3^{1,2} X_4^{0,1} X_5^0 \oplus X_4^{0,2} X_5^{1,2} \oplus X_3^2 X_4^1 X_5^1 \\
&= (X_3^0 \oplus X_3^1 \oplus X_3^2)(X_4^1)(X_5^0 \oplus X_5^2) \oplus (X_3^1 \oplus X_3^2)(X_4^0 \oplus X_4^1)(X_5^0) \\
&\quad \oplus (X_3^0 \oplus X_3^1 \oplus X_3^2)(X_4^0 \oplus X_4^2)(X_5^1 \oplus X_5^2) \oplus (X_3^2)(X_4^1)(X_5^1) \\
&= X_3^0 X_4^0 X_5^1 \oplus X_3^0 X_4^0 X_5^2 \oplus X_3^0 X_4^1 X_5^0 \oplus X_3^0 X_4^1 X_5^2 \oplus X_3^0 X_4^2 X_5^1 \oplus X_3^0 X_4^2 X_5^2 \oplus X_3^1 X_4^0 X_5^0 \oplus X_3^1 X_4^0 X_5^1 \oplus X_3^1 X_4^0 X_5^2 \\
&\quad \oplus X_3^1 X_4^1 X_5^2 \oplus X_3^2 X_4^0 X_5^0 \oplus X_3^2 X_4^1 X_5^1 \oplus X_3^2 X_4^2 X_5^1 \oplus X_3^2 X_4^2 X_5^2
\end{aligned}$$

Minterm	$X_3^0 X_4^0 X_5^0$	$X_3^0 X_4^0 X_5^1$	$X_3^0 X_4^0 X_5^2$	$X_3^0 X_4^1 X_5^0$	$X_3^0 X_4^1 X_5^1$	$X_3^0 X_4^1 X_5^2$	$X_3^0 X_4^2 X_5^0$	$X_3^0 X_4^2 X_5^1$	$X_3^0 X_4^2 X_5^2$
Input	0	1	1	1	0	1	0	1	1
Minterm	$X_3^1 X_4^0 X_5^0$	$X_3^1 X_4^0 X_5^1$	$X_3^1 X_4^0 X_5^2$	$X_3^1 X_4^1 X_5^0$	$X_3^1 X_4^1 X_5^1$	$X_3^1 X_4^1 X_5^2$	$X_3^1 X_4^2 X_5^0$	$X_3^1 X_4^2 X_5^1$	$X_3^1 X_4^2 X_5^2$
Input	1	1	1	0	0	1	0	0	0
Minterm	$X_3^2 X_4^0 X_5^0$	$X_3^2 X_4^0 X_5^1$	$X_3^2 X_4^0 X_5^2$	$X_3^2 X_4^1 X_5^0$	$X_3^2 X_4^1 X_5^1$	$X_3^2 X_4^1 X_5^2$	$X_3^2 X_4^2 X_5^0$	$X_3^2 X_4^2 X_5^1$	$X_3^2 X_4^2 X_5^2$
Input	1	0	0	0	1	0	0	1	1

Table 22: The inputs to the butterfly diagram, in Example 15, for the function F_3 , which are based on the minterms.

The inputs represent the coefficients of the minterms, listed in natural order. The minterms form the input to the butterfly, which is listed in Table 22, where a value of 1 is inputted if the corresponding minterm appears in the XOR of the minterms expression above, and a value of 0 if not. For instance, the number corresponding to the minterm $X_3^1 X_4^0 X_5^1$ is 1 because the minterm is in the expression, but the number corresponding to $X_3^1 X_4^2 X_5^1$ is 0 because the minterm is not in the expression.

The butterfly diagram is formed from n columns for each variable in descending order. The first column corresponds to the polarity Q_5 for the variable X_5 . The first column repeats the single-variable butterfly diagram for Q_5 for every three (3^1) rows (repeated nine times).

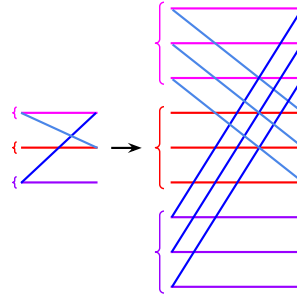


Figure 29: Process to create part of the column for Q_4 in Example 15.

The second column corresponds to the polarity Q_4 for the variable X_4 , and repeats a butterfly diagram kernel for every nine (3^2) rows. This butterfly diagram kernel is derived from the single-variable butterfly diagram for the polarity Q_4 . This part is altered to fit nine rows in the method demonstrated in Fig. 29. This kernel is repeated three times.

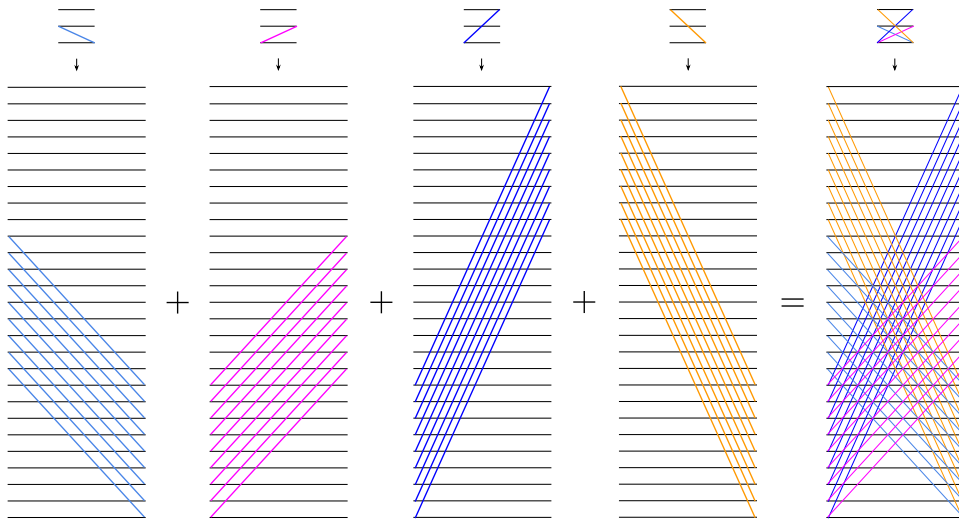


Figure 30: Process to create column for Q_3 in Example 15.

The third column corresponds to the polarity Q_3 for the variable X_3 . The butterfly diagram for this column is altered from the single-variable diagram for Q_3 , as illustrated in Fig. 30.

Combining all three columns yields the butterfly diagram shown in Fig. 31a for transforming any function of three ternary variables to the polarity Q_3, Q_4, Q_5 .

The outputs represent the spectral coefficients of the polarity terms, listed in natural order. The input for F_3 in the butterfly diagram leads to the MVI-FPRM

$$\begin{aligned}
 F_3 &= Q_3^1 Q_4^1 Q_5^2 \oplus Q_3^2 Q_4^3 Q_5^1 \oplus Q_3^3 Q_4^2 Q_5^3 \\
 &= X_3^{1,2} X_4^{0,1} \oplus X_3^{0,2} X_5^{1,2} \oplus X_4^1 X_5^{0,1}
 \end{aligned}$$

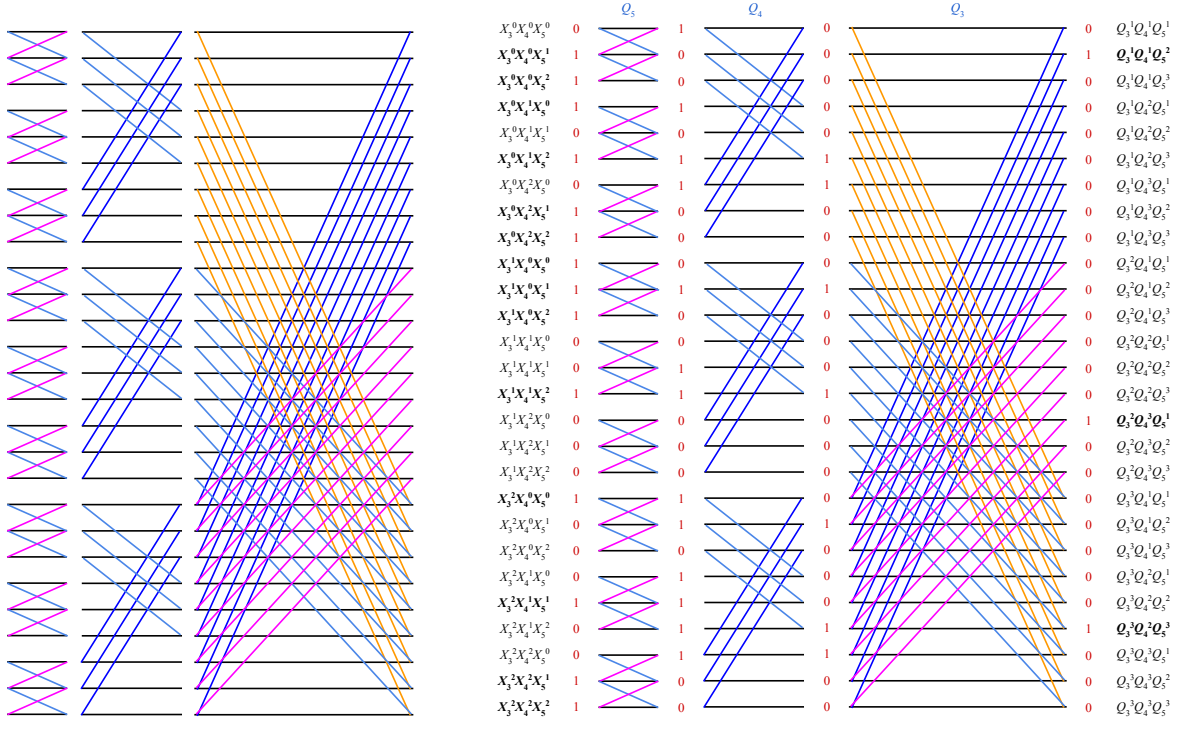


Figure 31: Full butterfly diagram for the polarity Q_3, Q_4, Q_5 , from Example 15.

as illustrated in Fig. 31b. This is the same MVI-FPRM as the one found in Example 10.

8 Circuit Synthesis Based on MVI-GRM

The method for MVI-GRM selects one of the top results from the MVI-FPRM method and utilizes factorization and transformation rules to determine the quasi-minimal MVI-GRM. In the multi-output MVI-FPRM, the same literals or even products are repeated for various outputs; therefore, they can be shared in the final circuit. However, in MVI-GRM, the method may create non-repeated literals and products that cannot be shared. This method is demonstrated in Example 16.

Example 16. The MVI-FPRM forms $F_1 = 1 \oplus X_2^2 \oplus X_1^{2,3} \oplus X_1^{2,3} X_2 \oplus X_1^{1,2,3} \oplus X_1^{1,2,3} X_2^2$ (from Example 4), $F_2 = 1 \oplus X_1^{2,3} \oplus X_1^{1,2,3} \oplus X_1^{2,3} X_2^2$ (from Example 6) were selected in the first phase, where the variable X_1 is quaternary and X_2 is ternary. Both of these forms can be factorized to create MVI-GRM forms, which are realized as circuits in Fig. 32. The circuit for F_1 has a Maslov cost of 13 and a TQC of 57, and the circuit for F_2 has the same Maslov and TQC cost.

$$\begin{aligned}
 F_1 &= 1 \oplus X_2^2 \oplus X_1^{2,3} \oplus X_1^{2,3} X_2^2 \oplus X_1^{1,2,3} \oplus X_1^{1,2,3} X_2^2 \\
 &= (1 \oplus X_1^{2,3} \oplus X_1^{1,2,3})(1 \oplus X_2^2) \\
 &= X_1^{0,2,3} X_2^{0,1} \\
 F_2 &= 1 \oplus X_1^{2,3} \oplus X_1^{1,2,3} \oplus X_1^{2,3} X_2^2 \\
 &= (1 \oplus X_1^{1,2,3}) \oplus X_1^{2,3} (1 \oplus X_2^2) \\
 &= X_1^0 \oplus X_1^{2,3} X_2^{0,1}
 \end{aligned}$$

If, instead, the functions $F_1 = \bar{x}_{2a} \oplus \bar{x}_{1a}x_{1b}\bar{x}_{2a}$ and $F_2 = \bar{x}_{1a}\bar{x}_{1b} \oplus x_{1a}\bar{x}_{2a}$ were realized as binary ESOP-based circuits, then the result would be the circuits shown in Fig. 33. The circuit for F_1 has a Maslov cost of 16 and a TQC of 125, and the circuit for F_2 is the same as the MVI-GRM-based circuit. Comparisons between the MVI-GRM-based circuits and ESOP-based circuits are summarized in Table 23.

Function	MVI-GRM-Based						ESOP-Based					
	NOT	CNOT	3-bit Toffoli	4-bit Toffoli	Maslov Cost	TQC	NOT	CNOT	3-bit Toffoli	4-bit Toffoli	Maslov Cost	TQC
F_1	3	0	2	0	13	57	2	1	0	1	16	125
F_2	3	0	2	0	13	57	3	0	2	0	13	57

Table 23: GRM-based vs ESOP-based circuits for F_1 and F_2 .

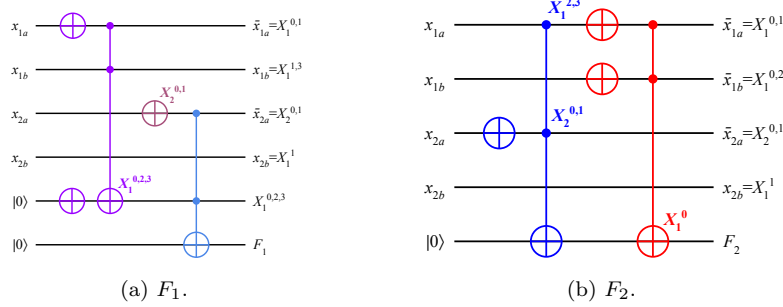


Figure 32: The circuits for F_1 and F_2 based on MVI-GRM, from Example 16.

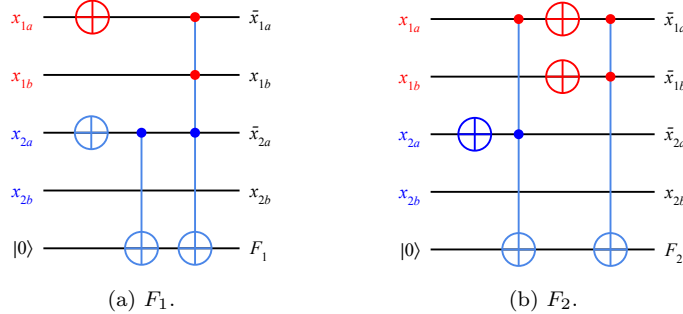


Figure 33: The circuits for F_1 and F_2 based on ESOP, from Example 16.

9 Conclusions

Two new types of binary quantum circuits are introduced in this paper, both based on multi-valued input, binary output (MVI) logic. We introduced the MVI-FPRM and MVI-GRM canonical forms. Two methods are presented for the synthesis of exact or approximate MVI-FPRM. The first method is based on products-matching, and the second method is based on our new MVI butterfly diagrams. MVI-GRM synthesis is based on the factorization of the selected-best MVI-FPRM with subsequent use of simplifying rules. In circuit synthesis based on MVI-FPRM, the same products are repeated in several outputs, so they can be reused, as achieved using polarity-based decoders for the MVI function, which aids the synthesis of multi-output functions. However, in MVI-GRM, non-repeated literals and products are created, which does not allow for sharing sub-functions. This is a typical trade-off with MVI-FPRM and MVI-GRM. Although this paper only deals with completely specified functions, it will be extended to incompletely specified functions in future papers. Our future work focuses on selecting variables for pairing and choosing the best decoders for a given Boolean function.

References

- [1] A. Javadi-Abhari, M. Treinish, K. Krsulich, C. J. Wood, J. Lishman, J. Gacon, S. Martiel, P. D. Nation, L. S. Bishop, A. W. Cross, *et al.*, “Quantum computing with qiskit,” *arXiv preprint arXiv:2405.08810*, 2024.
- [2] B. Schmitt, M. Soeken, G. De Micheli, and A. Mishchenko, “Scaling-up ESOP synthesis for quantum compilation,” in *IEEE 49th International Symposium on Multiple-Valued Logic*, pp. 13–18, IEEE, 2019.
- [3] A. Mishchenko and M. Perkowski, “Fast heuristic minimization of exclusive-sums-of-products,” in *5th International Workshop on Applications of the Reed Muller Expansion in Circuit Design*, 2001.
- [4] K. Fazel, M. A. Thornton, and J. E. Rice, “ESOP-based Toffoli gate cascade generation,” in *IEEE Pacific Rim Conference on Communications, Computers and Signal Processing*, pp. 206–209, IEEE, 2007.
- [5] G. Meuli, M. Soeken, M. Roetteler, N. Wiebe, and G. De Micheli, “A best-fit mapping algorithm to facilitate ESOP-decomposition in Clifford+T quantum network synthesis,” in *23rd Asia and South Pacific Design Automation Conference*, pp. 664–669, IEEE, 2018.
- [6] G. Meuli, B. Schmitt, R. Ehlers, H. Riener, and G. De Micheli, “Evaluating ESOP optimization methods in quantum compilation flows,” in *International Conference on Reversible Computation*, pp. 191–206, Springer, 2019.
- [7] J. Rice, K. Fazel, M. Thornton, and K. Kent, “Toffoli gate cascade generation using ESOP minimization and QMDD-based swapping,” in *Proceedings of the 2009 Reed-Muller Workshop*, pp. 63–72, 2009.
- [8] J. Rice and N. Nayeem, “Ordering techniques for ESOP-based Toffoli cascade generation,” in *Proceedings of 2011 IEEE Pacific Rim Conference on Communications, Computers and Signal Processing*, pp. 274–279, IEEE, 2011.
- [9] N. M. Nayeem and J. E. Rice, “A shared-cube approach to ESOP-based synthesis of reversible logic,” *Facta universitatis-series: Electronics and Energetics*, vol. 24, no. 3, pp. 385–402, 2011.

[10] D. Maslov and G. W. Dueck, “Reversible cascades with minimal garbage,” *IEEE Transactions on Computer-Aided Design of Integrated Circuits and Systems*, vol. 23, no. 11, pp. 1497–1509, 2004.

[11] J.-H. R. Jiang, G. De Micheli, K. Smith, and M. Soeken, “Design and automation for quantum computation and quantum technologies,” *IEEE Journal on Emerging and Selected Topics in Circuits and Systems*, vol. 12, no. 3, pp. 581–583, 2022.

[12] M. Saeedi and I. L. Markov, “Synthesis and optimization of reversible circuits—a survey,” *ACM Comput. Surv.*, vol. 45, Mar. 2013.

[13] R. Drechsler, B. Becker, and N. Göckel, “A genetic algorithm for minimization of fixed polarity Reed-Muller expressions,” in *Artificial Neural Nets and Genetic Algorithms: Proceedings of the International Conference in Alès, France, 1995*, pp. 393–395, Springer, 1995.

[14] A. Sarabi and M. Perkowski, “Fast exact and quasi-minimal minimization of highly testable fixed-polarity AND/XOR canonical networks,” in *Proceedings of 29th ACM/IEEE Design Automation Conference*, pp. 30–35, IEEE, 1992.

[15] D. Maslov and G. W. Dueck, “Improved quantum cost for n-bit Toffoli gates,” *Electronics Letters*, vol. 39, no. 25, pp. 1790–1791, 2003.

[16] A. Al-Bayaty and M. Perkowski, “GALA-n: Generic architecture of layout-aware n-bit quantum operators for cost-effective realization on IBM quantum computers,” *arXiv e-prints*, 2023.

[17] A. Al-Bayaty, X. Song, and M. Perkowski, “CALA-n: A Quantum Library for Realizing Cost-Effective 2-, 3-, 4-, and 5-bit Gates on IBM Quantum Computers using Bloch Sphere Approach, Clifford+T Gates, and Layouts,” *arXiv e-prints*, 2024.

[18] D. Debnath and T. Sasao, “GRMIN2: A heuristic simplification algorithm for generalised Reed-Muller expressions,” *IEE Proceedings-Computers and Digital Techniques*, vol. 143, no. 6, pp. 376–384, 1996.

[19] K. Dill and M. Perkowski, “Minimization of generalized Reed-Muller forms with a genetic algorithm,” *Proceedings of Genetic Programming*, vol. 97, 1997.

[20] K. M. Dill and M. A. Perkowski, “Baldwinian learning utilizing genetic and heuristic algorithms for logic synthesis and minimization of incompletely specified data with generalized Reed-Muller (AND-EXOR) forms,” *Journal of Systems Architecture*, vol. 47, no. 6, pp. 477–489, 2001.

[21] M. Helliwell and M. Perkowski, “A fast algorithm to minimize multi-output mixed-polarity generalized Reed-Muller forms,” in *Proceedings of the 25th ACM/IEEE Design automation conference*, pp. 427–432, 1988.

[22] T. Sasao, “Input variable assignment and output phase optimization of PLA’s,” *IEEE Transactions on Computers*, vol. C-33, no. 10, pp. 879–894, 1984.

[23] M. Perkowski, M. Helliwell, and P. Wu, “Minimization of multiple-valued input multi-output mixed-radix exclusive sums of products for incompletely specified Boolean functions,” in *Proceedings 19th Int. Symp. on Multiple-Valued Logic*, pp. 256–263, 1989.

[24] I. Schäfer and M. A. Perkowski, “Multiple-valued generalized Reed-Muller forms,” in *Proceedings Int. Symp. on Multiple-Valued Logic*, pp. 40–48, 1991.

[25] D. Green, “Families of Reed-Muller canonical forms,” *International Journal of Electronics Theoretical and Experimental*, vol. 70, no. 2, pp. 259–280, 1991.

[26] C. E. Shannon, “The synthesis of two-terminal switching circuits,” *The Bell System Technical Journal*, vol. 28, no. 1, pp. 59–98, 1949.

[27] M. Davio, J.-P. Deschamps, and A. Thayse, *Discrete and Switching Functions*. McGraw-Hill, 1978.

[28] M. AbuGhanem, “Tbm quantum computers: evolution, performance, and future directions,” *The Journal of Supercomputing*, vol. 81, p. 687, 2025.

[29] G. Rüdiger and A. Brandenburg, “A solar dynamo in the overshoot layer: cycle period and butterfly diagram.,” *Astronomy and Astrophysics*, v. 296, p. 557, vol. 296, p. 557, 1995.

[30] C. J. Weinstein, “Quantization effects in digital filters,” tech. rep., MIT Lincoln Laboratory, 1969.

[31] J. L. Shanks, “Computation of the fast Walsh-Fourier transform,” *IEEE Transactions on Computers*, vol. 100, no. 5, pp. 457–459, 1969.

[32] K. A. Vahid, A. Prabhu, A. Farhadi, and M. Rastegari, “Butterfly transform: An efficient fft based neural architecture design,” in *2020 IEEE/CVF conference on computer vision and pattern recognition (CVPR)*, pp. 12021–12030, IEEE, 2020.

[33] B. J. Falkowski and S. Yan, “Matrix decomposition and butterfly diagrams for mutual relations between hadamard-haar and arithmetic spectra,” *IEEE Transactions on Circuits and Systems I: Regular Papers*, vol. 53, no. 5, pp. 1119–1129, 2006.

[34] L. Li, M. Thornton, and M. Perkowski, “A quantum CAD Accelerator based on Grover’s algorithm for finding the minimum Fixed Polarity Reed-Muller form,” in *36th International Symposium on Multiple-Valued Logic (ISMVL ’06)*, pp. 33–33, IEEE, 2006.

[35] K. Jin, T. Soffat, J. Morgan, and M. Perkowski, “A polarity-based approach for optimization of multivalued quantum multiplexers with arbitrary single-qubit target gates,” *Journal of Applied Logics-IfCoLog Journal of Logics and their Applications*, vol. 7, no. 1, 2020.

- [36] M. Ilyas, S. Cui, and M. Perkowski, “Ternary logic design in topological quantum computing,” *Journal of Physics A: Mathematical and Theoretical*, vol. 55, p. 305302, jul 2022.
- [37] T. Sasao, “An exact minimization of AND-EXOR expressions using reduced covering functions,” in *Proceedings of the Synthesis and Simulation Meeting and International Interchange*, pp. 374–383, 1993.
- [38] L. Csank, M. Perkowski, and I. Schaefer, “Canonical restricted mixed-polarity exclusive-OR sums of products and the efficient algorithm for their minimisation,” *IEE Proceedings E (Computers and Digital Techniques)*, vol. 140, no. 1, pp. 69–77, 1993.
- [39] A. Kazimirov and V. Maleyev, “Genetic algorithm for minimization of ESOP representations for multiple-output logic functions,” in *Journal of Physics: Conference Series*, vol. 1847, p. 012028, IOP Publishing, 2021.
- [40] G. Papakonstantinou, “Exclusive or sum of complex terms expressions minimization,” *Integration*, vol. 56, pp. 44–52, 2017.
- [41] H. Riener, R. Ehlers, B. d. O. Schmitt, and G. D. Micheli, “Exact synthesis of ESOP forms,” in *Advanced Boolean Techniques: Selected Papers from the 13th International Workshop on Boolean Problems*, pp. 177–194, Springer, 2019.
- [42] H. B. Song, “A study on minimization algorithm for ESOP of multiple-valued function,” in *The Transactions of the Korea Information Processing*, 1997.
- [43] L. K. Grover, “A fast quantum mechanical algorithm for database search,” in *Proceedings of the twenty-eighth annual ACM symposium on Theory of Computing*, pp. 212–219, 1996.
- [44] A. Al-Bayaty and M. Perkowski, “BHT-QAOA: The generalization of quantum approximate optimization algorithm to solve arbitrary boolean problems as hamiltonians,” *Entropy*, vol. 26, no. 10, 2024.
- [45] A. S. H. Alasow, *Quantum search algorithms for constraint satisfaction and optimization problems using Grover’s search and quantum walk algorithms With advanced oracle design*. Portland State University, 2024.
- [46] J. Wakerly, *Digital Design: Principles and Practices*. Prentice Hall Xilinx design series, Prentice Hall, 1999.
- [47] N. Song and M. Perkowski, “Minimization of exclusive sum-of-products expressions for multiple-valued input, incompletely specified functions,” *IEEE Transactions on Computer-Aided Design of Integrated Circuits and Systems*, vol. 15, no. 4, pp. 385–395, 1996.
- [48] S. Roman, *Advanced linear algebra*. Springer, 2005.
- [49] B. Lee and M. Perkowski, “Quantum machine learning based on minimizing Kronecker-Reed-Muller forms and Grover search algorithm with hybrid oracles,” in *Euromicro Conference on Digital System Design (DSD)*, pp. 413–422, 2016.